



**HAL**  
open science

## 3D formulation of mono-symmetrical composite beams with deformable connection

Yassir Wardi, Pisey Keo, Mohammed Hjiaj

► **To cite this version:**

Yassir Wardi, Pisey Keo, Mohammed Hjiaj. 3D formulation of mono-symmetrical composite beams with deformable connection. *Finite Elements in Analysis and Design*, 2024, 237, pp.104163. 10.1016/j.finel.2024.104163 . hal-04570512

**HAL Id: hal-04570512**

**<https://univ-rennes.hal.science/hal-04570512>**

Submitted on 7 May 2024

**HAL** is a multi-disciplinary open access archive for the deposit and dissemination of scientific research documents, whether they are published or not. The documents may come from teaching and research institutions in France or abroad, or from public or private research centers.

L'archive ouverte pluridisciplinaire **HAL**, est destinée au dépôt et à la diffusion de documents scientifiques de niveau recherche, publiés ou non, émanant des établissements d'enseignement et de recherche français ou étrangers, des laboratoires publics ou privés.



Distributed under a Creative Commons Attribution - NonCommercial - NoDerivatives 4.0  
International License

# 3D formulation of mono-symmetrical composite beams with deformable connection

Yassir Wardi<sup>a,1</sup>, Pisey Keo<sup>a</sup>, Mohammed Hjiiaj<sup>a</sup>

<sup>a</sup>*Univ Rennes - INSA de Rennes, LGCGM/Structural Engineering Research Group, EA 3913, 20 avenue des Buttes de Coësmes, F-, 35700, Rennes, France*

---

## Abstract

This paper deals with a 3D linear formulation for mono-symmetric composite beams with deformable connection, taking into account non-uniform torsion. To simplify the development of the analytical solution, it is assumed that the warping of each layer of the composite section has no contribution on the stress resultants of each layer. Therefore, the warping function obtained with the classical St-Venant beam theory can be used for each subsection. As a result, the variables associated to both connection shearing plans become uncoupled. Using the virtual work principle, the governing equations are derived, and solved in closed-form. Based on the analytical expressions of the displacement fields, the exact stiffness matrix of the composite beam is computed. In addition, a displacement-based formulation is suggested. Appropriate polynomial interpolation functions are selected to circumvent slip-locking phenomenon. It has been shown that the slip-locking can be avoided by using quadratic shape function for axial displacement interpolations, by providing an additional middle node in each layer. Four examples are investigated in this paper. The prediction as well as the performance of the proposed direct stiffness method, are compared against an existing solution from the literature. In addition, slip-locking problem is addressed and the performance of the displacement-based method against the exact formulation is evaluated. The influence of warping effects on the composite beam response is assessed. Finally, a parametric study is conducted to evaluate the influence of connection rigidity and the coupling of the displacement fields on slip distributions.

*Keywords:* Composite beam, Direct stiffness method, interpolation functions, Slip, Locking

---

## 1. Introduction

Composite structures are one of the efficient solutions that shape the construction industry of the past decades, paving the way to innovation and advancement in the field of structural design and construction materials. Composite systems have become increasingly popular among the engineering, architectural and research communities who are investigating new alternative of high-performance structures. Choosing the appropriate materials, the strength-to-weight ratio of the structure may increase. Additionally, the use of composite structures such as steel-concrete, timber-steel or timber-concrete structures may decrease the carbon footprint of the buildings. That is a strong argument in promoting the development of environmentally sustainable solutions. Steel-concrete and concrete-timber are the typical applications of two-layered composite beams, which are normally formed by connecting two distinct beams through adhesive agents or mechanical devices. Usually, friction at the interface is not taken into account in force transfer mechanisms between the two layers. The connection is often assumed to be flexible, and become approximately rigid when using strong adhesive agents that limit the interface-slip. Regarding the modelling of the connections, a discrete or a continuous bond model can be used. Choosing the appropriate connection model is not simple, as the spacing of the connectors can significantly impact the results. In fact, in case of sparse connectors (with large spacing), using a continuous bond model can lead to a substantial underestimation of the deflection compared to the discrete model [1]. However, the continuous connection model was considered by Newmark [2] whose work has pioneered the consideration of a partial interaction in planar composite beams producing more realistic responses compared to the earlier rigid connection model. Thereafter, numerous studies [3, 4, 5, 6, 7, 8, 9, 10, 11, 12] have been conducted in order to investigate different aspects, aiming to produce more high performance 2D composite beam theories. In contrast to a large amount of research on 2D composite beam, 3D composite

---

*Email address:* [yassir.wardi@insa-rennes.fr](mailto:yassir.wardi@insa-rennes.fr) (Yassir Wardi)

beam receives less attention. Schnabl and Planinc [13] have developed a 3D beam theory assuming uniform torsion. They have extended the 2D theory to account for bi-axial bending, as well as torsion. Dall'Asta [14] has investigated two-layered composite beams with deformable connection under general loading conditions, taking into account non-uniform warping effects by adopting Vlasov assumptions. In case of composite beams, Dall'Asta [14] pointed out that the warping function depends on the shear modulus of both layers and the axial stiffness of the connection. Finding an analytical expression for the composite warping function, proves to be a challenging task, and it is not addressed in the present work.

The purpose of this paper is to present a new 3D formulation for a mono-symmetric composite beams. The kinematics of the composite beam are established using two local reference frames attached to the shear center of each layer. The connection at the interface consists in rows of connectors placed on the contact surface where slip can occur in two directions: longitudinal and lateral directions. The warping function of the composite beam is assumed to be independent of the contact interaction. This assumption may lead to a conservative result since the contribution of the connection rigidity to the torsional stiffness associated with warping is neglected. Indeed, it results in a larger slip at the interface. Using the virtual work principle, the strong-form of the equilibrium equations are derived along with consistent boundary conditions. Next, the governing equations are solved analytically. This paper also addresses the use of interpolation functions and their limitations in reproducing the results obtained with the closed-form solution. In fact, when a high connection stiffness value is used, the composite beam model produces a poor curvature description, which indicates the occurrence of the locking-problem. In the literature, this issue of slip-locking in 2D composite beam element has been extensively studied. Schnabl et al. [15] have introduced the modified virtual principle as an alternative for developing a shear and slip locking-free two-layered Timoshenko beam formulation. On the other hand, Dall'Asta and Zona [16] demonstrated that increasing the element with more degrees of freedom can enhance the accuracy of the element response. Studies conducted in [17] and [18] also confirmed that the use of more degrees of freedom improves the beam response. In

this paper, the same remedy is adopted.

This paper will be organized as follows. In section (2) the composite beam kinematics are described and the model assumptions are presented. In section (3), the composite beam equilibrium equations are derived using the principle of virtual work. The linear cross-section constitutive laws are recalled in section (4). The closed-form solution of the governing equations, as well as the exact stiffness of the composite element and the corresponding nodal forces are derived in section (5). Section (6) introduces the displacement-based formulation as an alternative to the direct stiffness method to derive the element stiffness matrix. Slip-locking issue is discussed in section (7), along with a proposal to achieve a locking-free formulation. Examples are discussed in section (8) to validate the proposed direct stiffness method and to highlight the performance of the displacement-based method compared to the direct formulation with regards to slip-locking issue. Finally, conclusions are drawn in section (9).

## 2. Beam Kinematics

### 2.1. Assumptions

The following assumptions are made for the development of the present composite beam formulation:

- (H1) - Each layer of the composite beam is homogeneous and isotropic;
- (H2) - The cross-section of each layer remains rigid in its own plane;
- (H3) - The vertical separation between the two layers is ignored;
- (H4) - The deformation and rotations are assumed to be small;
- (H5) - The two layers are connected by several rows of connectors placed longitudinally with respect to the composite section's plane of symmetry;
- (H6)- Without warping, plane section remains plane and orthogonal to the deformed beam axis during deformation (Eurler-Bernoulli beam theory);
- (H7)- The axial displacement due to torsion (warping effect) is proportional to the twist angle gradient (Vlasov theory);

(H8)- The warping of each layer has no contribution to the stress resultants at any cross-section.

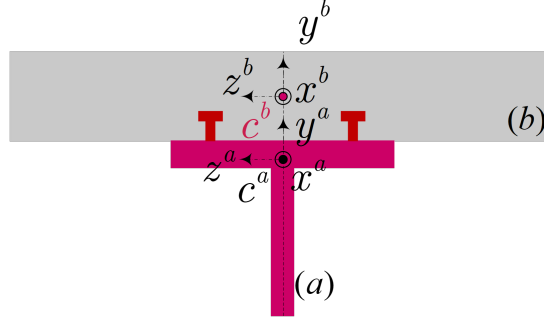


Figure 1: The composite beam section

## 2.2. Displacement field

The composite cross-section of the beam is composed of layer (a) and (b) that are connected by distributed connectors on their mutual contact surface as illustrated in fig. 1. Each layer has its own coordinate system located at its shear center.

Let  $\mathbf{e}_\alpha^k = (\mathbf{e}_x^k, \mathbf{e}_y^k, \mathbf{e}_z^k)$  be the orthonormal reference base of the beam ( $k$ ) in the initial configuration. The axis of the beam ( $k$ ) is presented by the base vector  $\mathbf{e}_x^k$ . The beam ( $k$ ) cross-section is then in the plane described by the base vectors  $(\mathbf{e}_y^k, \mathbf{e}_z^k)$ . The position of any arbitrary point  $P^k$  (see fig. 2) in the initial configuration can be expressed as:

$$\mathbf{X}^k = \mathbf{X}_c^k + y_c^k \mathbf{e}_y^k + z_c^k \mathbf{e}_z^k \quad (1)$$

where  $\mathbf{X}_c^k$  denotes the position vector of the shear center  $c^k$  of the beam ( $k$ ) in the initial configuration and  $(y_c^k, z_c^k)$  are the coordinates of point  $P^k$  with respect to the shear center. The deformed configuration of the beam ( $k$ ) is defined by the triad  $\mathbf{t}_\alpha^k = (\mathbf{t}_x^k, \mathbf{t}_y^k, \mathbf{t}_z^k)$ , which form a right-handed orthogonal basis according to the Euler-Bernoulli assumption (H6). Following (H2), (H6) and (H7), the position of the point  $P^k$  in the deformed configuration is then given by:

$$\mathbf{x}^k = \mathbf{x}_c^k + y_c^k \mathbf{t}_y^k + z_c^k \mathbf{t}_z^k + u_\omega^k(x^k, y_c^k, z_c^k) \mathbf{t}_x^k \quad (2)$$

where

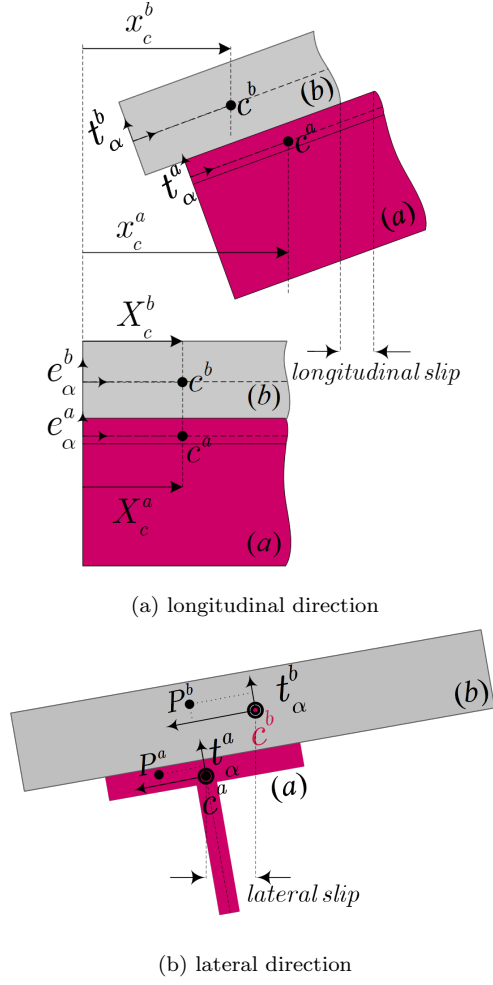


Figure 2: Deformed configuration

- $u_\omega^k(x^k, y_c^k, z_c^k)$  denotes the longitudinal displacement generated by warping;
- $\mathbf{x}_c^k$  denotes the position vector of the shear center  $c^k$  in the deformed configuration of the beam ( $k$ ).

The two bases  $\mathbf{e}_\alpha^k$  and  $\mathbf{t}_\alpha^k$  in the initial and deformed configuration are related by an orthogonal rotation matrix  $\mathbf{R}^k$  such that:

$$\mathbf{t}_\alpha^k = \mathbf{R}^k \mathbf{e}_\alpha^k \quad (3)$$

Recalling the Euler-Rodrigues formula for the rotation matrix in [19],  $\mathbf{R}^k$  can be expressed as:

$$\mathbf{R}^k = \cos(\varphi^k)\mathbf{I}_3 + \frac{\sin(\varphi^k)}{\varphi^k}\hat{\boldsymbol{\theta}}^{kc} + \frac{1 - \cos(\varphi^k)}{(\varphi^k)^2}\boldsymbol{\theta}^{kc}\boldsymbol{\theta}^{kcT} \quad (4)$$

with  $\boldsymbol{\theta}^{kc} = \begin{bmatrix} \theta_x^{kc} & \theta_y^{kc} & \theta_z^{kc} \end{bmatrix}^T$  being 3D rotation vector about the shear center of beam ( $k$ ),  $\hat{\boldsymbol{\theta}}^{kc}$  the skew-matrix which is defined as the cross-product of the vector  $\boldsymbol{\theta}^{kc}$  with an arbitrary vector, and  $\varphi^k = \|\boldsymbol{\theta}^{kc}\|$  its corresponding angle. Considering the small rotation hypothesis (H4), the first order approximation of the rotation matrix eq. (4) is given by:

$$\mathbf{R}^k = \mathbf{I}_3 + \hat{\boldsymbol{\theta}}^{kc} = \begin{bmatrix} 1 & -\theta_z^{kc} & \theta_y^{kc} \\ \theta_z^{kc} & 1 & -\theta_x^{kc} \\ -\theta_y^{kc} & \theta_x^{kc} & 1 \end{bmatrix} \quad (5)$$

Subtracting eq. (1) from eq. (2) and making use of eq. (3), one obtains the displacement field:

$$\mathbf{d}^k = \mathbf{d}_c^k + y_c^k (\mathbf{R}^k - \mathbf{I}_3) \mathbf{e}_y^k + z_c^k (\mathbf{R}^k - \mathbf{I}_3) \mathbf{e}_z^k + u_\omega^k(x^k, y_c^k, z_c^k) \mathbf{R}^k \mathbf{e}_x^k \quad (6)$$

with  $\mathbf{d}_c^k = \mathbf{x}_c^k - \mathbf{X}_c^k = u_c^k \mathbf{e}_x^k + v_c^k \mathbf{e}_y^k + w_c^k \mathbf{e}_z^k$ .

Neglecting the non-linear terms in eq. (6), the displacement field can be expressed as:

$$u^k = u_c^k - y_c^k \theta_z^{kc} + z_c^k \theta_y^{kc} + u_\omega^k \quad (7a)$$

$$v^k = v_c^k - z_c^k \theta_x^{kc} \quad (7b)$$

$$w^k = w_c^k + y_c^k \theta_x^{kc} \quad (7c)$$

where  $(u^k, v^k, w^k)$  are the components of the displacement vector  $\mathbf{d}^k$  in the direction of  $x$ -,  $y$ - and  $z$ -axis, respectively, and  $(u_c^k, v_c^k, w_c^k)$  are the corresponding displacements of the shear center.

The longitudinal displacement due to warping, according to Vlasov kinematic assumption (H7), can be expressed as:

$$u_\omega^k(x^k, y_c^k, z_c^k) = \omega^k(y_c^k, z_c^k) \theta_{x,x}^{kc} \quad (8)$$

where  $(\bullet)_{,x}$  denotes the derivative of  $(\bullet)$  with respect to  $x$ . Within the hypothesis made in (H8),  $\omega^k$  represents the warping function with respect to the shear center of beam ( $k$ )

cross-section and fulfills the following normality conditions:

$$\int E^k \omega^k dA^k = 0; \int E^k y_g^k \omega^k dA^k = 0; \int E^k z_g^k \omega^k dA^k = 0; k = \{a, b\} \quad (9)$$

where  $(y_g^k, z_g^k)$  are the coordinates of an arbitrary point on the cross-section, with respect to the centroid of the beam ( $k$ ).

The kinematics, described in eq. (7), can be formulated in the reference base with origin attached to the centroid of each cross-section. To do so, it is necessary to perform the following change of variables:

$$y_c^k = y_g^k - c_y^k \quad (10a)$$

$$z_c^k = z_g^k - c_z^k \quad (10b)$$

where  $(c_y^k, c_z^k)$  are the coordinates of the shear center in the new coordinates system  $(y_g^k, z_g^k)$ . In case of mono-symmetrical cross-sections,  $c_z^k = 0$  for  $k = \{a, b\}$ . Therefore, the beam kinematics can be expressed as follows:

$$u^k = u_c^k + c_y^k \theta_z^{kc} - y_g^k \theta_z^{kc} + z_g^k \theta_y^{kc} + \omega^k \theta_{x,x}^{kc} \quad (11a)$$

$$v^k = v_c^k - z_g^k \theta_x^{kc} \quad (11b)$$

$$w^k = w_c^k + (y_g^k - c_y^k) \theta_x^{kc} \quad (11c)$$

To fulfill the hypothesis made in (H8), the axial displacement of the shear center has to be related to the axial displacement of the beam centroid through the following expression:

$$u_c^k = u_0^k - c_y^k \theta_z^{kc} \quad (12)$$

Inserting eq. (12) into eq. (11), the beam kinematics can be reformulated as:

$$u^k = u_0^k - y_g^k \theta_z^k + z_g^k \theta_y^k + \omega^k \theta_{x,x}^k \quad (13a)$$

$$v^k = v_c^k - z_g^k \theta_x^k \quad (13b)$$

$$w^k = w_c^k + (y_g^k - c_y^k) \theta_x^k \quad (13c)$$

in which we denote  $\theta_x^k = \theta_x^{kc}$ ,  $\theta_y^k = \theta_y^{kc}$  and  $\theta_z^k = \theta_z^{kc}$  to simplify the notation. Considering Euler-Bernoulli assumption, we have:  $\theta_y^k = -w_{c,x}^k$  and  $\theta_z^k = v_{c,x}^k$ .

In what follows, for the sake of simplicity, the subscript  $(\cdot)_g$  representing the coordinate system referring to the centroid of the cross-section is omitted.

### 2.3. Slip at interface

The inter-layer slip is considered in both directions: a longitudinal slip in the  $x$ -axis of the beam and a lateral slip in the  $z$ -axis direction due to the transverse plane deformation of the composite beam. In case of using  $2n$ -row connectors ( $n$ -row on either side of symmetric axis of the composite cross-section), there are  $2n + 1$  slips:  $2n$  longitudinal slips and one lateral slip.

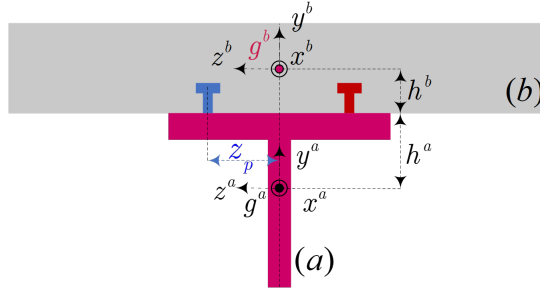


Figure 3: The connectors position

For a row of connectors ( $p$ ), located at  $z_p$  with respect to the reference axis of the beam ( $a$ ) see fig. 3, the slip is defined as:

$$\mathbf{s}_p = \mathbf{d}_p^a(x, h^a, z_p) - \mathbf{d}_p^b(x, -h^b, z_p) \quad (14)$$

where  $\mathbf{d}_p^k$  represents the displacement field of an arbitrary point on the contact surface of the beam ( $k$ ) for  $k = \{a, b\}$ . The slip components can be obtained by inserting eq. (13) into eq. (14) as:

$$s_{px} = -\Delta u_0 - h^a \theta_z^a - h^b \theta_z^b - z_p \Delta \theta_y + \omega_p^a \frac{\partial \theta_x^a}{\partial x} - \omega_p^b \frac{\partial \theta_x^b}{\partial x} \quad (15a)$$

$$s_{py} = -\Delta v_c + z_p \Delta \theta_x \quad (15b)$$

$$s_{pz} = -\Delta w_c + h^a \theta_x^a + h^b \theta_x^b - c_y^a \theta_x^a + c_y^b \theta_x^b \quad (15c)$$

with  $\Delta(\cdot) = (\cdot)^b - (\cdot)^a$ ,  $\omega_p^a = \omega^a (h^a - c_y^a, z_p)$  and  $\omega_p^b = \omega^b (-h^b - c_y^b, z_p)$ . It can be seen that the lateral slip  $s_{pz}$  is independent of the connector position  $z_p$ . As a result, there is only one lateral slip  $s_z$  to be considered in the model.

The no-uplift condition (H3) imposes that:

$$s_{py} = -\Delta v_c + z_p \Delta \theta_x = 0 \quad (16)$$

The eq. (16) holds true for any position  $z_p$  of the connectors, thus:

$$\Delta v_c = 0; \Delta \theta_x = 0 \quad (17)$$

Therefore, both beams exhibit the same vertical displacement ( $v_c = v_c^a = v_c^b$ ) and the same twist angle ( $\theta_x = \theta_x^a = \theta_x^b$ ). Consequently, the composite beam's kinematics can be simplified to the following:

$$u^k = u_0^k - y_g^k \theta_z + z_g^k \theta_y^k + \omega^k \theta_{x,x} \quad (18a)$$

$$v^k = v_c - z_g^k \theta_x \quad (18b)$$

$$w^k = w_c^k + (y_g^k - c_y^k) \theta_x \quad (18c)$$

with  $\theta_z = \theta_z^a = \theta_z^b = v_{c,x}$ . Taking into account the constraints given in eq. (17) and eq. (18), the slip components can be evaluated as follows:

$$s_{px} = -\Delta u_0 - h \theta_z - z_p \Delta \theta_y + \omega_p \theta_{x,x} \quad (19a)$$

$$s_z = -\Delta w_c + h_c \theta_x \quad (19b)$$

where  $\omega_p = \omega^a (h^a - c_y^a, z_p) - \omega^b (-h^b - c_y^b, z_p)$ ,  $h = h^a + h^b$  and  $h_c = h - c_y^a + c_y^b$ .

#### 2.4. Strain field

By using the composite beam kinematics, the linear strain can be evaluated as:

$$\varepsilon_x^k = u_{,x}^k = u_{0,x}^k - y^k \theta_{z,x} + z^k \theta_{y,x}^k + \omega^k \theta_{x,xx} \quad (20a)$$

$$\gamma_{xy}^k = u_{,y}^k + v_{,x}^k = (\omega_{,y}^k - z^k) \theta_{x,x} \quad (20b)$$

$$\gamma_{xz}^k = u_{,z}^k + w_{,x}^k = (\omega_{,z}^k + y^k - c_y^k) \theta_{x,x} \quad (20c)$$

### 3. Equilibrium condition

The equilibrium condition of the composite beam possessing  $2n$ -row of connectors is derived on the basis of the virtual work principle. Using the displacement fields developed in eq. (18) and eq. (19), we can express the balance between the work done by external and internal forces for an arbitrary virtual displacement. The beam is supposed to be subjected to external loading consisting of uniform distributed loads  $\mathbf{f}_u^k$  with  $k = \{a, b\}$ , and concentrated forces and moments  $\mathbf{Q}_n$ . Thus, the virtual work principle for the composite beam can be formulated as:

$$\sum_{k=a,b} \int_{V^k} (\sigma_x^k \delta \varepsilon_x^k + \tau_{xy}^k \delta \gamma_{xy}^k + \tau_{xz}^k \delta \gamma_{xz}^k) dV^k + \int_0^L \mathbf{D}_{sc}^T \delta \mathbf{d}_{sc} dx = \sum_{k=a,b} \int_{V^k} \mathbf{f}_u^k{}^T \delta \mathbf{d}_u^k dx + \delta \mathbf{q}^T \mathbf{Q}_n \quad (21)$$

where:

- $\sigma_x^k$ ,  $\tau_{xy}^k$  and  $\tau_{xz}^k$  are the axial and the shear stresses acting on the beam ( $k$ ) cross-section;
- $\delta \varepsilon_x^k$ ,  $\delta \gamma_{xy}^k$  and  $\delta \gamma_{xz}^k$  are, respectively their corresponding virtual strains;
- $\mathbf{D}_{sc}^T \delta \mathbf{d}_{sc}$  is the virtual work done by the shear forces in the connection at the interface i.e.:  $\mathbf{D}_{sc}^T \delta \mathbf{d}_{sc} = \sum_{p=1}^{2n} D_{px}^{sc} \delta s_{px} + D_z^{sc} \delta s_z$ ;
- $\mathbf{f}_u^k{}^T \delta \mathbf{d}_u^k$  is the virtual work done by the uniform distributed external loads of beam ( $k$ ) where

$$\delta \mathbf{d}_u^k = [\delta u_0^k, \delta v_c, \delta w_c^k, \delta \theta_x, \delta \theta_y^k, \delta \theta_z, \delta \theta_{x,x}]^T$$

$$\mathbf{f}_u^k = [n_x^k, q_y^k, q_z^k, m_x^k, m_y^k, m_z^k, b_x^k]^T$$

- $\mathbf{q}$  is the nodal displacements of the composite beam element given by:

$$\mathbf{q} = [\mathbf{q}_0^T, \mathbf{q}_L^T]^T$$

with

$$\mathbf{q}_0 = [u_0^a(0), u_0^b(0), v_c(0), w_c^a(0), w_c^b(0), \theta_x(0), \theta_y^a(0), \theta_y^b(0), \theta_z(0), \theta_{x,x}(0)]^T$$

$$\mathbf{q}_L = [u_0^a(L), u_0^b(L), v_c(L), w_c^a(L), w_c^b(L), \theta_x(L), \theta_y^a(L), \theta_y^b(L), \theta_z(L), \theta_{x,x}(L)]^T$$

As illustrated in Figure 4,  $\mathbf{q}_0$  and  $\mathbf{q}_L$  represent the composite beam's degrees of freedom at the element ends. Introducing eqs. (13), (19) and (20) into eq. (21), we get:

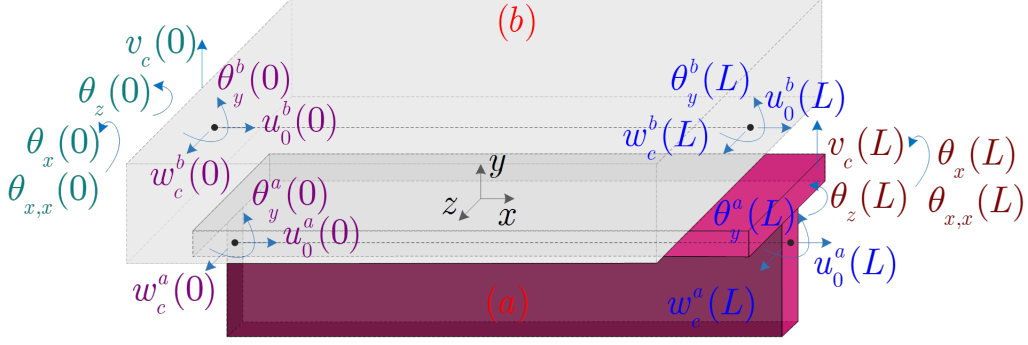


Figure 4: The composite beam's degrees of freedom

$$\int_0^L \mathbf{D}^T \hat{\boldsymbol{\delta}} (\delta \mathbf{d}) dx + \int_0^L \mathbf{D}_{sc}^T \hat{\boldsymbol{\delta}}_{sc} (\delta \mathbf{d}) dx = \sum_{k=a,b} \int_{V^k} \mathbf{f}_u^k{}^T \delta \mathbf{d}_u^k dx + \delta \mathbf{q}^T \mathbf{Q}_n \quad (22)$$

where:

$$\delta \mathbf{d} = [\delta u_0^a, \delta u_0^b, \delta v_c, \delta w_c^a, \delta w_c^b, \delta \theta_x]^T$$

$$\mathbf{D} = [N^a, N^b, M_z, M_y^a, M_y^b, M_x, B]^T$$

$$\mathbf{D}_{sc} = [D_{1x}^{sc}, D_{2x}^{sc}, \dots, D_{2nx}^{sc}, D_z^{sc}]^T$$

$$\hat{\boldsymbol{\delta}} = \begin{bmatrix} \frac{\partial}{\partial x} & 0 & 0 & 0 & 0 & 0 & 0 \\ 0 & \frac{\partial}{\partial x} & 0 & 0 & 0 & 0 & 0 \\ 0 & 0 & \frac{\partial^2}{\partial x^2} & 0 & 0 & 0 & 0 \\ 0 & 0 & 0 & -\frac{\partial^2}{\partial x^2} & 0 & 0 & 0 \\ 0 & 0 & 0 & 0 & -\frac{\partial^2}{\partial x^2} & 0 & 0 \\ 0 & 0 & 0 & 0 & 0 & \frac{\partial}{\partial x} & \frac{\partial^2}{\partial x^2} \end{bmatrix}^T$$

$$\hat{\mathbf{d}}_{sc} = \begin{bmatrix} 1 & 1 & \dots & 1 & 0 \\ -1 & -1 & \dots & -1 & 0 \\ -h \frac{\partial}{\partial x} & -h \frac{\partial}{\partial x} & \dots & -h \frac{\partial}{\partial x} & 0 \\ -z_1 \frac{\partial}{\partial x} & -z_2 \frac{\partial}{\partial x} & \dots & -z_{2n} \frac{\partial}{\partial x} & -1 \\ z_1 \frac{\partial}{\partial x} & z_2 \frac{\partial}{\partial x} & \dots & z_{2n} \frac{\partial}{\partial x} & -1 \\ \omega_1 \frac{\partial}{\partial x} & \omega_2 \frac{\partial}{\partial x} & \dots & \omega_{2n} \frac{\partial}{\partial x} & h_c \end{bmatrix}^T$$

in which:  $N^k = \int_{A^k} \sigma_x^k dA$ ;  $M_x = \sum_{k=a,b,A^k} \int \left[ \tau_{xy}^k \left( \frac{\partial \omega^k}{\partial y} - z^k \right) + \tau_{xz}^k \left( \frac{\partial \omega^k}{\partial z} + y^k - c_y^k \right) \right] dA$ ;  $M_y^k = \int_{A^k} z^k \sigma_x^k dA$ ;  $M_z = - \sum_{k=a,b,A^k} \int y^k \sigma_x^k dA$ ; and  $B = \sum_{k=a,b,A^k} \int \sigma_x^k \omega^k dA$ .

Performing integration by parts, we can rewrite the principle of virtual work as follows:

$$\delta \mathbf{q}^T (\mathbf{Q} - \mathbf{Q}_{ext}) - \int_0^L \delta \mathbf{d}^T \left( \tilde{\mathbf{d}} \mathbf{D} + \tilde{\mathbf{d}}_{sc} \mathbf{D}_{sc} + \tilde{\mathbf{d}}_e \mathbf{Q}_e \right) dx = 0 \quad (23)$$

where:

$$\mathbf{Q}_e = \left[ n_x^a, n_x^b, q_y^a + q_y^b, q_z^a, q_z^b, m_x^a + m_x^b, m_y^a, m_y^b, m_z^a + m_z^b, b_x^a + b_x^b \right]^T,$$

$$\tilde{\mathbf{d}} = \begin{bmatrix} \frac{\partial}{\partial x} & 0 & 0 & 0 & 0 & 0 & 0 \\ 0 & \frac{\partial}{\partial x} & 0 & 0 & 0 & 0 & 0 \\ 0 & 0 & -\frac{\partial^2}{\partial x^2} & 0 & 0 & 0 & 0 \\ 0 & 0 & 0 & \frac{\partial^2}{\partial x^2} & 0 & 0 & 0 \\ 0 & 0 & 0 & 0 & \frac{\partial^2}{\partial x^2} & 0 & 0 \\ 0 & 0 & 0 & 0 & 0 & \frac{\partial}{\partial x} & -\frac{\partial^2}{\partial x^2} \end{bmatrix},$$

$$\tilde{\mathbf{d}}_{sc} = \begin{bmatrix} -1 & -1 & \dots & -1 & 0 \\ 1 & 1 & \dots & 1 & 0 \\ -h \frac{\partial}{\partial x} & -h \frac{\partial}{\partial x} & \dots & -h \frac{\partial}{\partial x} & 0 \\ -z_1 \frac{\partial}{\partial x} & -z_2 \frac{\partial}{\partial x} & \dots & -z_{2n} \frac{\partial}{\partial x} & -1 \\ z_1 \frac{\partial}{\partial x} & z_2 \frac{\partial}{\partial x} & \dots & z_{2n} \frac{\partial}{\partial x} & 1 \\ \omega_1 \frac{\partial}{\partial x} & \omega_2 \frac{\partial}{\partial x} & \dots & \omega_{2n} \frac{\partial}{\partial x} & -h_c \end{bmatrix},$$

$$\tilde{\boldsymbol{\delta}}_e = \begin{bmatrix} 1 & 0 & 0 & 0 & 0 & 0 & 0 & 0 & 0 & 0 \\ 0 & 1 & 0 & 0 & 0 & 0 & 0 & 0 & 0 & 0 \\ 0 & 0 & 1 & 0 & 0 & 0 & 0 & 0 & -\frac{\partial}{\partial x} & 0 \\ 0 & 0 & 0 & 1 & 0 & 0 & \frac{\partial}{\partial x} & 0 & 0 & 0 \\ 0 & 0 & 0 & 0 & 1 & 0 & 0 & \frac{\partial}{\partial x} & 0 & 0 \\ 0 & 0 & 0 & 0 & 0 & 1 & 0 & 0 & 0 & -\frac{\partial}{\partial x} \end{bmatrix}.$$

Equation (23) being satisfied for all admissible variations, we can derive the following equilibrium equations:

$$\tilde{\boldsymbol{\delta}}\mathbf{D} + \tilde{\boldsymbol{\delta}}_{sc}\mathbf{D}_{sc} + \tilde{\boldsymbol{\delta}}_e\mathbf{Q}_e = \mathbf{0} \quad (24)$$

and the following natural boundary conditions:

$$\mathbf{Q} - \mathbf{Q}_{ext} = \mathbf{0} \quad (25)$$

The expanded forms of eq. (24) can be expressed as:

$$N_{,x}^a - \sum_{p=1}^{2n} D_{px}^{sc} + n_x^a = 0 \quad (26a)$$

$$N_{,x}^b + \sum_{p=1}^{2n} D_{px}^{sc} + n_x^b = 0 \quad (26b)$$

$$-M_{z,xx} - \sum_{p=1}^{2n} h D_{px,x}^{sc} + q_y^a + q_y^b - m_{z,x}^a - m_{z,x}^b = 0 \quad (26c)$$

$$M_{y,xx}^a - \sum_{p=1}^{2n} z_p D_{px,x}^{sc} - D_z^{sc} + q_z^a + m_{y,x}^a = 0 \quad (26d)$$

$$M_{y,xx}^b + \sum_{p=1}^{2n} z_p D_{px,x}^{sc} + D_z^{sc} + q_z^b + m_{y,x}^b = 0 \quad (26e)$$

$$M_{x,x} - B_{,xx} + \sum_{p=1}^{2n} \omega_p D_{px,x}^{sc} - h_c D_z^{sc} + m_x^a + m_x^b - b_{x,x}^a - b_{x,x}^b = 0 \quad (26f)$$

and the natural boundary conditions are:

$$\begin{aligned}
N^a(0) &= -Q_1; & N^a(L) &= Q_{11}; \\
N^b(0) &= -Q_2; & N^b(L) &= Q_{12}; \\
-M_{z,x}(0) - h \sum_{p=1}^{2n} D_{px}^{sc}(0) - m_z(0) &= -Q_3; & -M_{z,x}(L) - h \sum_{p=1}^{2n} D_{px}^{sc}(L) - m_z(L) &= Q_{13}; \\
M_{y,x}^a(0) - \sum_{p=1}^{2n} z_p D_{px}^{sc}(0) + m_y^a(0) &= -Q_4; & M_{y,x}^a(L) - \sum_{p=1}^{2n} z_p D_{px}^{sc}(L) + m_y^a(L) &= Q_{14}; \\
M_{y,x}^b(0) + \sum_{p=1}^{2n} z_p D_{px}^{sc}(0) + m_y^b(0) &= -Q_5; & M_{y,x}^b(L) + \sum_{p=1}^{2n} z_p D_{px}^{sc}(L) + m_y^b(L) &= Q_{15}; \\
M_x(0) - B_{,x}(0) + \sum_{p=1}^{2n} \omega_p D_{px}^{sc}(0) + b_x(0) &= -Q_6; & M_x(L) - B_{,x}(L) + \sum_{p=1}^{2n} \omega_p D_{px}^{sc}(L) + b_x(L) &= Q_{16}; \\
M_y^a(0) &= -Q_7; & M_y^a(L) &= Q_{17}; \\
M_y^b(0) &= -Q_8; & M_y^b(L) &= Q_{18}; \\
M_z(0) &= -Q_9; & M_z(L) &= Q_{19}; \\
B(0) &= -Q_{10}; & B(L) &= Q_{20};
\end{aligned}$$

in which  $Q_1$  to  $Q_{20}$  are applied nodal forces and moments.

#### 4. Constitutive laws

For linear and isotropic material, the axial and shear stresses of beam can be related to the linear strains as:

$$\sigma_x^k = E^k \varepsilon_x^k \quad (27a)$$

$$\tau_{xy}^k = G^k \gamma_{xy}^k \quad (27b)$$

$$\tau_{xz}^k = G^k \gamma_{xz}^k \quad (27c)$$

where  $E^k$  and  $G^k$  are the Young and shear modulus of the beam ( $k$ ), respectively. For every connector row ( $p$ ),  $K_{px}$  and  $K_z$  represent, respectively, the uniformly distributed connection

stiffness for axial and lateral slips. The constitutive law for the connection is linear. Thus, the contact forces and slips can be related as follows:

$$D_{px}^{sc} = K_{px} s_{px} \quad (28a)$$

$$D_z^{sc} = K_z s_z \quad (28b)$$

Combining the kinematics given in eqs. (19) and (20) and the constitutive laws provided in the eqs. (27) and (28), the internal forces can be formulated as follows:

$$N^k = E^k A^k u_{0,x}^k \quad (29a)$$

$$M_y^k = E^k I_y^k \theta_{y,x}^k \quad (29b)$$

$$M_z = \overline{EI}_z^s \theta_{z,x} \quad (29c)$$

$$M_x = \overline{GJ}^s \theta_{x,x} \quad (29d)$$

$$B = \overline{EI}_\omega^s \theta_{x,xx} \quad (29e)$$

$$D_{px}^{sc} = K_{px} (-\Delta u_0 - h \theta_z - z_p \Delta \theta_y + \omega_p \theta_{x,x}) \quad (29f)$$

$$D_z^{sc} = K_z (-\Delta w_c + h_c \theta_x) \quad (29g)$$

where  $I_y^k = \int_{A^k} (z^k)^2 dA$ ;  $I_z^k = \int_{A^k} (y^k)^2 dA$ ;  $I_x^k = \int_{A^k} [(y^k)^2 + (z^k)^2] dA$ ;  $I_\omega^k = \int_{A^k} (\omega^k)^2 dA$ ;  $C_t^k = \int_{A^k} [z^k \omega_{,y}^k - (y^k - c_y^k) \omega_{,z}^k] dA$ ;  $J^k = I_x^k + (c_y^k)^2 A^k - C_t^k$ ;  $\overline{EI}_z^s = E^a I_z^a + E^b I_z^b$ ;  $\overline{GJ}^s = G^a J^a + G^b J^b$ ; and  $\overline{EI}_\omega^s = E^a I_\omega^a + E^b I_\omega^b$ .

The linear constitutive laws eq. (29) can be cast in the compact forms as:

$$\mathbf{D} = \mathbf{K}_m \hat{\boldsymbol{\theta}} \mathbf{d} \quad (30)$$

and

$$\mathbf{D}_{sc} = \mathbf{K}_{sc} \hat{\boldsymbol{\theta}}_{sc} \mathbf{d} \quad (31)$$

where

$$\mathbf{K}_m = \begin{bmatrix} E^a A^a & 0 & 0 & 0 & 0 & 0 & 0 \\ 0 & E^b A^b & 0 & 0 & 0 & 0 & 0 \\ 0 & 0 & \overline{EI}_z^s & 0 & 0 & 0 & 0 \\ 0 & 0 & 0 & E^a I_y^a & 0 & 0 & 0 \\ 0 & 0 & 0 & 0 & E^b I_y^b & 0 & 0 \\ 0 & 0 & 0 & 0 & 0 & \overline{GJ}^s & 0 \\ 0 & 0 & 0 & 0 & 0 & 0 & \overline{EI}_\omega^s \end{bmatrix}; \mathbf{K}_{sc} = \begin{bmatrix} K_{1x} & 0 & \dots & 0 & 0 \\ 0 & K_{2x} & \dots & 0 & 0 \\ \vdots & \vdots & \ddots & 0 & 0 \\ 0 & 0 & \dots & K_{2nx} & 0 \\ 0 & 0 & 0 & 0 & K_z \end{bmatrix}$$

## 5. Direct stiffness method

In the direct stiffness method, the equilibrium equations are written in terms of the composite beam's displacements which are analytically solved. From the analytical solutions, all expressions of all mechanical variables are determined and the internal forces are obtained via the force-displacement relationship of the composite beam. Next, the composite element stiffness matrix can be derived along with its corresponding nodal forces.

### 5.1. Displacement fields

The solution of the governing equations provides the expressions of all the displacement field. The latter is obtained by combining the beam kinematics developed in section 2, the equilibrium equations (26) and the constitutive relations (29). Inserting eq. (29) into

eq. (26), we get:

$$E^a A^a u_{0,xx}^a + 2 \sum_{p=1}^n K_{px} (\Delta u_0 + h \theta_z) + n_x^a = 0 \quad (32a)$$

$$E^b A^b u_{0,xx}^b - 2 \sum_{p=1}^n K_{px} (\Delta u_0 + h \theta_z) + n_x^b = 0 \quad (32b)$$

$$\overline{EI}_z^s \theta_{z,xxx}^a - 2h \sum_{p=1}^n K_{px} (\Delta u_{0,x} + h \theta_{z,x}) = q_y^a + q_y^b - m_{z,x}^a - m_{z,x}^b \quad (32c)$$

$$E^a I_y^a \theta_{y,xxx}^a + K_z (\Delta w_c - h_c \theta_x) + 2 \sum_{p=1}^n K_{px} (z_p^2 \Delta \theta_{y,x} - z_p \omega_p \theta_{x,xx}) + q_z^a + m_{y,x}^a = 0 \quad (32d)$$

$$E^b I_y^b \theta_{y,xxx}^b - K_z (\Delta w_c - h_c \theta_x) - 2 \sum_{p=1}^n K_{px} (z_p^2 \Delta \theta_{y,x} - z_p \omega_p \theta_{x,xx}) + q_z^b + m_{y,x}^b = 0 \quad (32e)$$

$$\begin{aligned} \overline{GJ}_z^s \theta_{x,xxx} - \overline{EI}_\omega^s \theta_{x,xxxx} - h_c K_z (-\Delta w_c + h_c \theta_x) \\ + 2 \sum_{p=1}^n K_{px} (-z_p \omega_p \Delta \theta_{y,x} + \omega_p^2 \theta_{x,xx}) + m_x - b_{x,x} = 0 \end{aligned} \quad (32f)$$

in which the symmetry of connectors with respect to y-axis is considered.

It can be seen that in the system of equations (32), the variables in the XY-plane are uncoupled from the ones in the XZ-plane. This uncoupling feature is due to the assumption made in (H8). In what follows, the solution will be split into two parts. The first one will be reserved to the development of the solution for  $u_0^a$ ,  $u_0^b$  and  $\theta_z$  using eqs. (32a) to (32c), and the second part is the solution for  $w_c^a$ ,  $w_c^b$  and  $\theta_x$  using eqs. (32d) to (32f). It is worth mentioning that the solution will be derived under static external loading conditions and uniform shear connection stiffness:  $K_{xp} = K_x$ .

### 5.1.1. The XY-plane solution

The solution in the XY-plane is obtained by solving a differential equation with a single independent variable. The displacement fields are formulated on the basis of this sole variable.

Dividing eq. (32a) and eq. (32b) by  $E^a A^a$  and  $E^b A^b$ , respectively, and then subtracting the outcomes leads to the following:

$$-\Delta u_{0,xx} - \frac{2nK_x}{EA} g_u + \frac{n_x^a}{E^a A^a} - \frac{n_x^b}{E^b A^b} = 0 \quad (33)$$

where:  $g_u = -\Delta u_0 - h \theta_z$ ;  $\overline{EA}^s = E^a A^a + E^b A^b$  and  $\overline{EA} = \frac{E^a A^a E^b A^b}{\overline{EA}^s}$ .

Multiplying eq. (32c) with  $(-\frac{h}{\overline{EI}_z^s})$  and adding the result to the derivation of eq. (33), we obtain the governing equation in the  $XY$ -plane as:

$$g_{u,xxx} - 2nK_x \left( \frac{1}{\overline{EA}} + \frac{h^2}{\overline{EI}_z^s} \right) g_{u,x} + \frac{h(q_y^a + q_y^b)}{\overline{EI}_z^s} = 0 \quad (34)$$

whose solution is:

$$g_u = \mathbf{X}_{g_u} \mathbf{C}_u + Z_{g_u} \quad (35)$$

with:

$$\begin{aligned} \mathbf{X}_{g_u} &= [1, e^{\lambda_u(x-L)}, e^{-\lambda_u x}, 0, 0, 0, 0, 0]; & Z_{g_u} &= \frac{h(q_y^a + q_y^b)}{\lambda_u^2 \overline{EI}_z^s} x \\ \mathbf{C}_u &= [C_1, C_2, C_3, C_4, C_5, C_6, C_7, C_8]^T \quad \text{and} & \lambda_u^2 &= 2nK_x \left( \frac{1}{\overline{EA}} + \frac{h^2}{\overline{EI}_z^s} \right). \end{aligned}$$

The vector  $\mathbf{C}_u$  represents the integration constants. It is worth noting that for highly stiff longitudinal connection, the term  $e^{\lambda_u x}$  may go to infinity for any positive values of  $x$ . Hence, the term  $e^{\lambda_u(x-L)}$  whose values will range between 0 and 1 is introduced to address this numerical ill-conditioning problem.

Inserting the solution of  $g_u$  into eqs. (32a) and (32b) and performing double integration, we obtain:

$$u_0^a = \mathbf{X}_u^a \mathbf{C}_u + Z_u^a \quad (36a)$$

$$u_0^b = \mathbf{X}_u^b \mathbf{C}_u + Z_u^b \quad (36b)$$

with:

$$\begin{aligned} \mathbf{X}_u^a &= \frac{2nK_x}{E^a A^a} \int \left( \int \mathbf{X}_{g_u} dx \right) dx + x\mathbb{I}_4 + \mathbb{I}_5; & Z_u^a &= \frac{2nK_x}{E^a A^a} \int \left( \int Z_{g_u} dx \right) dx - \frac{n_x^a}{2E^a A^a} x^2 \\ \mathbf{X}_u^b &= -\frac{2nK_x}{E^b A^b} \int \left( \int \mathbf{X}_{g_u} dx \right) dx + x\mathbb{I}_6 + \mathbb{I}_7; & Z_u^b &= -\frac{2nK_x}{E^b A^b} \int \left( \int Z_{g_u} dx \right) dx - \frac{n_x^b}{2E^b A^b} x^2 \\ \mathbb{I}_4 &= \begin{bmatrix} 0 & 0 & 0 & 1 & 0 & 0 & 0 & 0 \end{bmatrix}; & \mathbb{I}_5 &= \begin{bmatrix} 0 & 0 & 0 & 0 & 1 & 0 & 0 & 0 \end{bmatrix} \\ \mathbb{I}_6 &= \begin{bmatrix} 0 & 0 & 0 & 0 & 0 & 1 & 0 & 0 \end{bmatrix}; & \mathbb{I}_7 &= \begin{bmatrix} 0 & 0 & 0 & 0 & 0 & 0 & 1 & 0 \end{bmatrix} \end{aligned}$$

Besides, by using the definition of  $g_u$ , the rotation  $\theta_z$  and the vertical displacement  $v_c$  can be expressed as follows:

$$\theta_z = \mathbf{X}_{\theta_z} \mathbf{C}_u + Z_{\theta_z} \quad (37a)$$

$$v_c = \mathbf{X}_{v_c} \mathbf{C}_u + Z_{v_c} \quad (37b)$$

where:

$$\begin{aligned} \mathbf{X}_{\theta_z} &= -\frac{1}{h} (\mathbf{X}_u^b - \mathbf{X}_u^a + \mathbf{X}_{g_u}); & Z_{\theta_z} &= -\frac{1}{h} (Z_u^b - Z_u^a + Z_{g_u}) \\ \mathbf{X}_{v_c} &= \int \mathbf{X}_{\theta_z} dx + \mathbb{I}_8; & Z_{v_c} &= \int Z_{\theta_z} dx \\ \mathbb{I}_8 &= \begin{bmatrix} 0 & 0 & 0 & 0 & 0 & 0 & 0 & 1 \end{bmatrix}. \end{aligned}$$

### 5.1.2. The XZ-plane solution

Similar to the previous development, the solution for the XZ-plane can be obtained by solving the coupled system of equations (32d-32f). The compact representation of the system of equations is firstly derived.

Subtracting eq. (32e) from eq. (32d), we get:

$$-\Delta w_{c,xxxx} + \frac{K_z}{EI_y} (-\Delta w_c + h_c \theta_x) + \frac{2K_x}{EI_y} \sum_{p=1}^n (z_p^2 \Delta w_{c,xx} + z_p \omega_p \theta_{x,xx}) + \frac{q_z^b}{E^b I_y^b} - \frac{q_z^a}{E^a I_y^a} = 0 \quad (38)$$

in which  $\theta_y^k = -w_{c,x}^k$  has been used. Equations (32f) and (38) can be cast in the following form:

$$\mathbf{A}_1 \mathbf{Y}_{w,xxxx} - \mathbf{A}_2 \mathbf{Y}_{w,xx} + \mathbf{A}_3 \mathbf{Y}_w = \mathbf{F}_w \quad (39)$$

where:

$$\begin{aligned} \mathbf{Y}_w &= [\Delta w_c, \theta_x]^T; & \overline{EI}_y &= \frac{E^a I_y^a E^b I_y^b}{E^a I_y^a + E^b I_y^b} \\ \mathbf{A}_1 &= \begin{bmatrix} \overline{EI}_y & 0 \\ 0 & \overline{EI}_\omega^s \end{bmatrix}; & \mathbf{A}_2 &= K_x \begin{bmatrix} 2 \sum_{p=1}^n z_p^2 & 2 \sum_{p=1}^n z_p \omega_p^{ab} \\ 2 \sum_{p=1}^n z_p \omega_p & \frac{\overline{GJ}^s}{K_x} + 2 \sum_{p=1}^n (\omega_p)^2 \end{bmatrix} \\ \mathbf{A}_3 &= K_z \begin{bmatrix} 1 & -h_c \\ -h_c & h_c^2 \end{bmatrix}; & \mathbf{F}_w &= \begin{bmatrix} \frac{\overline{EI}_y}{E^b I_y^b} q_z^b - \frac{\overline{EI}_y}{E^a I_y^a} q_z^a \\ m_x \end{bmatrix}. \end{aligned}$$

Assume that the solution of eq. (39) has the following form:

$$\mathbf{Y}_w = \mathbf{Y}_w^h + \mathbf{Y}_w^p = \mathbf{V}_e e^{rx} + \mathbf{Y}_w^p \quad (40)$$

where  $\mathbf{Y}_w^p$  represents the particular solution and  $\mathbf{Y}_w^h = \mathbf{V}_e e^{rx}$  the homogeneous solution of the system. Inserting eq. (40) into eq. (39), we obtain the corresponding eigenvalue problem as:

$$\mathbf{M}_e \mathbf{V}_e = \mathbf{0} \quad (41a)$$

$$\mathbf{A}_1 \mathbf{Y}_{w,xxxx}^p - \mathbf{A}_2 \mathbf{Y}_{w,xx}^p + \mathbf{A}_3 \mathbf{Y}_w^p = \mathbf{F}_w \quad (41b)$$

where  $\mathbf{M}_e = r^4 \mathbf{A}_1 - r^2 \mathbf{A}_2 + \mathbf{A}_3$ . The vector  $\mathbf{V}_e$  is therefore the eigenvector associated with the zero-eigenvalue of the matrix  $\mathbf{M}_e$ . To compute all possible solutions, it is necessary to find all  $r$  that verify:  $\det(\mathbf{M}_e) = 0$ . Consequently, the characteristic equation of the system can be expressed as follows:

$$\det(\mathbf{M}_e) = r^8 + a_6 r^6 + a_4 r^4 + a_2 r^2 = 0 \quad (42)$$

where:

$$a_4 = K_z \left( \frac{1}{EI_y} + \frac{h_c^2}{EI_\omega^s} \right) + K_x^2 \left( \frac{\overline{GJ}^s I_y^{sc}}{K_x} + I_y^{sc} I_\omega^{sc} - (I_{y\omega}^{sc})^2 \right) \frac{1}{EI_y EI_\omega^s};$$

$$a_6 = -K_x \left( \frac{\overline{GJ}^s}{K_x EI_\omega^s} + \frac{I_\omega^{sc}}{EI_\omega^s} + \frac{I_y^{sc}}{EI_y} \right)$$

$$a_2 = -K_z K_x \left( h_c^2 I_y^{sc} + \frac{\overline{GJ}^s}{K_x} + I_\omega^{sc} + 2 I_{y\omega}^{sc} h_c \right) \frac{1}{EI_y EI_\omega^s};$$

$$I_y^{sc} = 2 \sum_{p=1}^n z_p^2; \quad I_\omega^{sc} = 2 \sum_{p=1}^n \omega_p^2; \quad \text{and} \quad I_{y\omega}^{sc} = 2 \sum_{p=1}^n z_p \omega_p.$$

The eq. (42) is an octic polynomial characterized by eight roots. The roots can be real or complex numbers. A simple factorization shows that zero is a double root, which leaves only six of them to be identified. Considering the change of variable  $t = r^2$ , the characteristic equation can be transformed into a cubic polynomial, which makes finding the roots a lot easier, using Cardano's formula [20].

$$(t^3 + a_6 t^2 + a_4 t + a_2) t = 0 \quad (43)$$

The solution of eq. (43) provides four roots for  $t$ , resulting in eight conjugate complex numbers roots for  $r$ . Consequently, the roots of eq. (42) are:

$$\begin{cases} r_1 = 0; & r_2 = 0; \\ r_3 = \alpha; & r_4 = -\alpha; \\ r_5 = a + i b; & r_6 = a - i b; \\ r_7 = -a + i b; & r_8 = -a - i b \end{cases} \quad (44)$$

where  $\alpha$  can be either a real or complex number and  $a$  and  $b$  are real positive numbers. Hence, the homogeneous solution can be formulated as follows:

$$\begin{aligned} \mathbf{Y}_w^h &= \mathbf{V}_{e1} (C_9 + C_{10}x) + \mathbf{V}_{e3} (C_{11}e^{\alpha(x-L)} + C_{12}e^{-\alpha x}) \\ &+ C_{13} [\mathbf{R}_{e5} \cos(bx) - \mathbf{I}_{e5} \sin(bx)] e^{a(x-L)} + C_{14} [\mathbf{R}_{e5} \sin(bx) + \mathbf{I}_{e5} \cos(bx)] e^{a(x-L)} \\ &+ C_{15} [\mathbf{R}_{e5} \cos(bx) + \mathbf{I}_{e5} \sin(bx)] e^{-ax} + C_{16} [-\mathbf{R}_{e5} \sin(bx) + \mathbf{I}_{e5} \cos(bx)] e^{-ax} \end{aligned} \quad (45)$$

where:

- $\mathbf{V}_{e1}$  is the eigenvector corresponding to the eigenvalues  $r_1$  and  $r_2$ ;
- $\mathbf{V}_{e3}$  is the eigenvector corresponding to the eigenvalues  $r_3$  and  $r_4$ ;
- $\mathbf{R}_{e5}$  is the real part of the eigenvector associated to the eigenvalue  $r_5$ ;
- $\mathbf{I}_{e5}$  is the imaginary part of the eigenvector associated to the eigenvalue  $r_5$ ;
- $C_9$  to  $C_{16}$  are constants of integration.

It is worth mentioning that the solution depends on the values of parameters  $a_6$ ,  $a_4$  and  $a_2$  and it may be in a different form for other cases. Therefore, the closed-form expressions need to be updated accordingly. For the particular part of the solution  $\mathbf{Y}_w^p$ , we can assume the following form:

$$\mathbf{Y}_w^p = \frac{p_1}{2} x^2 \begin{bmatrix} h_c \\ 1 \end{bmatrix} + p_2 \begin{bmatrix} 0 \\ 1 \end{bmatrix} \quad (46)$$

where  $p_1$  and  $p_2$  are parameters to be determined. It is worth noting that the vector  $[h_c, 1]^T$  is the eigenvector associated to zero-eigenvalue of the matrix  $\mathbf{A}_3$  whose determinant is zero. So,  $\mathbf{Y}_w^p$  must verify eq. (41b) as:

$$-\mathbf{A}_2 \begin{bmatrix} h_c \\ 1 \end{bmatrix} p_1 + \mathbf{A}_3 \begin{bmatrix} 0 \\ 1 \end{bmatrix} p_2 = \mathbf{F}_w \quad (47)$$

which can be solved for  $p_1$  and  $p_2$ . Therefore, the solution of eq. (39) ( $\Delta w_c$  and  $\theta_x$ ) can be obtained as:

$$\mathbf{Y}_\omega(1) = \Delta w_c = w_c^b - w_c^a = \mathbf{X}_{\Delta w_c} \mathbf{C}_w + Z_{\Delta w_c} \quad (48)$$

$$\mathbf{Y}_\omega(2) = \theta_x = \mathbf{X}_{\theta_x} \mathbf{C}_w + Z_{\theta_x} \quad (49)$$

where

$$\begin{aligned} s_1 &= \mathbf{V}_{e1}(1); & s_5 &= [\mathbf{R}_{e5}(1) \cos(bx) - \mathbf{I}_{e5}(1) \sin(bx)] e^{a(x-L)} \\ s_2 &= \mathbf{V}_{e1}(1)x; & s_6 &= [\mathbf{R}_{e5}(1) \sin(bx) + \mathbf{I}_{e5}(1) \cos(bx)] e^{a(x-L)} \\ s_3 &= \mathbf{V}_{e3}(1)e^{\alpha(x-L)}; & s_7 &= [\mathbf{R}_{e5}(1) \cos(bx) + \mathbf{I}_{e5}(1) \sin(bx)] e^{-ax} \\ s_4 &= \mathbf{V}_{e3}(1)e^{-\alpha x}; & s_8 &= [-\mathbf{R}_{e5}(1) \sin(bx) + \mathbf{I}_{e5}(1) \cos(bx)] e^{-ax} \\ t_1 &= \mathbf{V}_{e1}(2); & t_5 &= [\mathbf{R}_{e5}(2) \cos(bx) - \mathbf{I}_{e5}(2) \sin(bx)] e^{a(x-L)} \\ t_2 &= \mathbf{V}_{e1}(2)x; & t_6 &= [\mathbf{R}_{e5}(2) \sin(bx) + \mathbf{I}_{e5}(2) \cos(bx)] e^{a(x-L)} \\ t_3 &= \mathbf{V}_{e3}(2)e^{\alpha(x-L)}; & t_7 &= [\mathbf{R}_{e5}(2) \cos(bx) + \mathbf{I}_{e5}(2) \sin(bx)] e^{-ax} \\ t_4 &= \mathbf{V}_{e3}(2)e^{-\alpha x}; & t_8 &= [-\mathbf{R}_{e5}(2) \sin(bx) + \mathbf{I}_{e5}(2) \cos(bx)] e^{-ax} \\ Z_{\Delta w_c} &= \frac{p_1 h_c}{2} x^2; & Z_{\theta_x} &= \frac{p_1}{2} x^2 + p_2 \end{aligned}$$

$$\mathbf{C}_w = [C_9, C_{10}, C_{11}, C_{12}, C_{13}, C_{14}, C_{15}, C_{16}, C_{17}, C_{18}, C_{19}, C_{20}]^T$$

$$\mathbf{X}_{\Delta w_c} = [s_1, s_2, s_3, s_4, s_5, s_6, s_7, s_8, 0, 0, 0, 0]$$

$$\mathbf{X}_{\theta_x} = [t_1, t_2, t_3, t_4, t_5, t_6, t_7, t_8, 0, 0, 0, 0].$$

Next, the remaining displacement fields are determined. Adding eq. (32d) to eq. (32e), we have:

$$E^a I_y^a w_{c,xxxx}^a + E^b I_y^b w_{c,xxxx}^b = q_z^a + q_z^b \quad (50)$$

Integrating eq. (50) four times, we get:

$$f_w = E^a I_y^a w_c^a + E^b I_y^b w_c^b = \frac{q_z^a + q_z^b}{24} x^4 + C_{17} \frac{1}{6} x^3 + C_{18} \frac{1}{2} x^2 + C_{19} x + C_{20} = \mathbf{X}_{f_w} \mathbf{C}_w + Z_{f_w} \quad (51)$$

where  $C_{17}$  to  $C_{20}$  are constants of integration. Combining eq. (51) with eq. (48) and solving for  $w_c^a$  and  $w_c^b$ , we gets:

$$w_c^a = \mathbf{X}_{w_c^a} \mathbf{C}_w + Z_{w_c^a} \quad (52)$$

$$w_c^b = \mathbf{X}_{w_c^b} \mathbf{C}_w + Z_{w_c^b} \quad (53)$$

and consequently,

$$\theta_y^a = \mathbf{X}_{\theta_y^a} \mathbf{C}_w + Z_{\theta_y^a} \quad (54)$$

$$\theta_y^b = \mathbf{X}_{\theta_y^b} \mathbf{C}_w + Z_{\theta_y^b} \quad (55)$$

where:

$$\begin{aligned} \mathbf{X}_{w_c^a} &= \mathbf{X}_{f_w} - \frac{E^b I_y^b}{E I_y^s} \mathbf{X}_{\Delta w_c}; & Z_{w_c^a} &= Z_{f_w} - \frac{E^b I_y^b}{E I_y^s} Z_{\Delta w_c} \\ \mathbf{X}_{w_c^b} &= \mathbf{X}_{f_w} + \frac{E^a I_y^a}{E I_y^s} \mathbf{X}_{\Delta w_c}; & Z_{w_c^b} &= Z_{f_w} + \frac{E^a I_y^a}{E I_y^s} Z_{\Delta w_c} \\ \mathbf{X}_{\theta_y^a} &= - \left( \frac{\partial \mathbf{X}_{f_w}}{\partial x} - \frac{E^b I_y^b}{E I_y^s} \frac{\partial \mathbf{X}_{\Delta w_c}}{\partial x} \right); & Z_{\theta_y^a} &= - \frac{\partial Z_{f_w}}{\partial x} + \frac{E^b I_y^b}{E I_y^s} \frac{\partial Z_{\Delta w_c}}{\partial x} \\ \mathbf{X}_{\theta_y^b} &= - \left( \frac{\partial \mathbf{X}_{f_w}}{\partial x} + \frac{E^a I_y^a}{E I_y^s} \frac{\partial \mathbf{X}_{\Delta w_c}}{\partial x} \right); & Z_{\theta_y^b} &= - \frac{\partial Z_{f_w}}{\partial x} - \frac{E^a I_y^a}{E I_y^s} \frac{\partial Z_{\Delta w_c}}{\partial x} \end{aligned}$$

### 5.2. Stress resultants

Once the displacement fields are determined, the internal forces can be obtained by using the linear elastic relationship eq. (29) as:

$$N^k = \mathbf{Y}_{N^k} \mathbf{C}_u + R_{N^k} \quad (56a)$$

$$M_y^k = \mathbf{Y}_{M_y^k} \mathbf{C}_w + R_{M_y^k} \quad (56b)$$

$$M_z = \mathbf{Y}_{M_z} \mathbf{C}_u + R_{M_z} \quad (56c)$$

$$M_x = \mathbf{Y}_{M_x} \mathbf{C}_w + R_{M_x} \quad (56d)$$

$$B = \mathbf{Y}_B \mathbf{C}_w + R_B \quad (56e)$$

$$D_{px}^{sc} = \mathbf{Y}_{D_{px}^{sc}}^u \mathbf{C}_u + R_{D_{px}^{sc}}^u + \mathbf{Y}_{D_{px}^{sc}}^w \mathbf{C}_w + R_{D_{px}^{sc}}^w \quad (56f)$$

$$D_z^{sc} = \mathbf{Y}_{D_z^{sc}} \mathbf{C}_w + R_{D_z^{sc}} \quad (56g)$$

where:

$$\mathbf{Y}_{N^k} = E^k A^k \frac{\partial \mathbf{X}_u^k}{\partial x}; \quad R_{N^k} = E^k A^k \frac{\partial Z_u^k}{\partial x}$$

$$\mathbf{Y}_{M_y^k} = E^k I_y^k \frac{\partial \mathbf{X}_{\theta_y^k}}{\partial x}; \quad R_{M_y^k} = E^k I_y^k \frac{\partial Z_{\theta_y^k}}{\partial x}$$

$$\mathbf{Y}_{M_z} = \overline{EI}_z^s \frac{\partial \mathbf{X}_{\theta_z}}{\partial x}; \quad R_{M_z} = \overline{EI}_z^s \frac{\partial Z_{\theta_z}}{\partial x}$$

$$\mathbf{Y}_{M_x} = \overline{GJ}^s \frac{\partial \mathbf{X}_{\theta_x}}{\partial x}; \quad R_{M_x} = \overline{GJ}^s \frac{\partial Z_{\theta_x}}{\partial x}$$

$$\mathbf{Y}_B = \overline{EI}_\omega^s \frac{\partial^2 \mathbf{X}_{\theta_x}}{\partial x^2}; \quad R_B = \overline{EI}_\omega^s \frac{\partial^2 Z_{\theta_x}}{\partial x^2}$$

$$\mathbf{Y}_{D_{px}^{sc}}^u = K_{px} [\mathbf{X}_u^a - \mathbf{X}_u^b - h \mathbf{X}_{\theta_z}]; \quad R_{D_{px}^{sc}}^u = K_{px} [Z_u^a - Z_u^b - h Z_{\theta_z}]$$

$$\mathbf{Y}_{D_{px}^{sc}}^w = K_{px} \left[ -z_p (\mathbf{X}_{\theta_y^b} - \mathbf{X}_{\theta_y^a}) + \omega_p \frac{\partial \mathbf{X}_{\theta_x}}{\partial x} \right]; \quad R_{D_{px}^{sc}}^w = K_{px} \left[ -z_p (Z_{\theta_y^b} - Z_{\theta_y^a}) + \omega_p \frac{\partial Z_{\theta_x}}{\partial x} \right]$$

$$\mathbf{Y}_{D_z^{sc}} = K_z (-\mathbf{X}_{\Delta w_c} + h_c \mathbf{X}_{\theta_x}); \quad R_{D_z^{sc}} = K_z (-Z_{\Delta w_c} + h_c Z_{\theta_x})$$

### 5.3. Direct stiffness matrix

The composite beam element possesses twenty degrees of freedom consistent with the ten displacement fields  $(u_0^a, u_0^b, v_c, w_c^a, w_c^b, \theta_x, \theta_y^a, \theta_y^b, \theta_{x,x})$  evaluated at  $x = 0$  and  $x = L$ . The displacement vector can be expressed as:

$$\mathbf{q} = \mathbf{X} \mathbf{C} + \mathbf{q}_z \quad (57)$$

where  $\mathbf{q}_z$  is the vector of the displacement associated with the external loads (particular solutions);  $\mathbf{X}$  is a constant matrix and  $\mathbf{C}$  is a vector collecting the twenty constants of integration. Similarly, the vector of internal nodal forces of the element can be formulated as:

$$\mathbf{Q} = \mathbf{Y} \mathbf{C} + \mathbf{R}_z \quad (58)$$

The stiffness matrix is determined based on expressing the nodal forces in terms of the displacement fields evaluated at end nodes. We proceed by eliminating the constants of integration. Since the nodal displacement are independent, the matrix  $\mathbf{X}$  is invertible. Hence, the constants of integration  $\mathbf{C}$  can be obtained as a function of the nodal displacements  $\mathbf{q}$  as:

$$\mathbf{C} = \mathbf{X}^{-1} (\mathbf{q} - \mathbf{q}_z) \quad (59)$$

Inserting eq. (59) into eq. (58), we obtain:

$$\mathbf{K}_e \mathbf{q} = \mathbf{Q} + \mathbf{Q}_0 \quad (60)$$

where

$$\mathbf{K}_e = \mathbf{Y} \mathbf{X}^{-1} \quad (61)$$

represents the beam element stiffness matrix and

$$\mathbf{Q}_0 = \mathbf{K} \mathbf{q}_z - \mathbf{R}_z \quad (62)$$

corresponds to the nodal forces due to the external loading.

## 6. Displacement based formulation

In this section, we derive the standard stiffness matrix of the composite beam element based on selected shape functions that approximate the element's displacement fields. To do so, Hermite interpolation functions are adopted for vertical and lateral displacements as well as for twisting angle, while either linear or quadratic polynomials can be used for the axial displacements. In 2D composite beams, it has been demonstrated that locking problems may occur in the displacement-based method if the linear approximation is adopted for

axial displacements. However, the use of quadratic polynomials resolves this issue [16]. Further details will be discussed in section 7.

Assume that the displacement fields is approximated as:

$$\mathbf{d} = \mathbf{N} \mathbf{q} \quad (63)$$

where  $\mathbf{N}$  is the shape function matrix. Inserting eqs. (30), (31) and (63) into eq. (22), we obtain:

$$\delta \mathbf{q}^T [\mathbf{K}_e \mathbf{q} - \mathbf{Q}_{ext}] = 0 \quad (64)$$

where

$$\mathbf{K}_e = \int_0^L \left[ \left( \hat{\partial} \mathbf{N} \right)^T \mathbf{K}_m \hat{\partial} \mathbf{N} + \left( \hat{\partial}_{sc} \mathbf{N} \right)^T \mathbf{K}_{sc} \hat{\partial}_{sc} \mathbf{N} \right] dx$$

is the element stiffness matrix and

$$\mathbf{Q}_{ext} = \int_0^L \mathbf{N}^T \tilde{\partial}_e \mathbf{Q}_e dx + \mathbf{Q}_n$$

is the element nodal force vector.

## 7. Locking problem

It has been shown that slip-locking is a numerical issue that impacts the performance of the displacement-based finite element model of 2D composite beam and can lead to erroneous results [16, 17, 18]. This issue is mainly related to the use of an inappropriate interpolation functions to describe the curvature and slip field in case of a highly stiff connection. In this section, we will demonstrate the roots of slip-locking and how to avoid it. Without losing generality, a mono-symmetrical composite section with a single row of connectors, placed along the axis of symmetry, is considered. With high connection stiffnesses, the slips would tend to zeros. The zero-slip state is characterized by the following:

$$- \Delta u_0 - h \theta_z = 0 \quad (65a)$$

$$- \Delta w_c + h \theta_x = 0 \quad (65b)$$

from which we can deduce the followings conditions:

$$\Delta u_0^i + h\theta_z^i = 0 \quad (66a)$$

$$\Delta w_c^i - h\theta_x^i = 0 \quad (66b)$$

$$\Delta w_c^j - h\theta_x^j = 0 \quad (66c)$$

$$\Delta\theta_y^i + h\theta_{x,x}^i = 0 \quad (66d)$$

$$\Delta\theta_y^j + h\theta_{x,x}^j = 0 \quad (66e)$$

where the superscript  $(\bullet)^i$  and  $(\bullet)^j$  represent the element end nodes. By adopting Hermitian interpolation functions for the vertical displacement and the twisting angle, and linear function for axial displacements,  $\Delta u_0$ ,  $\theta_z$ ,  $\Delta w_c$  and  $\theta_x$  can be expressed as follows:

$$\Delta u_0 = \left(1 - \frac{x}{L}\right) \Delta u_0^i + \frac{x}{L} \Delta u_0^j \quad (67a)$$

$$\theta_z = -\frac{6x}{L^2} v_c^i + \frac{6x}{L^2} v_c^j + \left(1 - \frac{4x}{L}\right) \theta_z^i - \frac{2x}{L} \theta_z^j + \frac{3x^2}{L^2} \left(\theta_z^i + \theta_z^j - 2\frac{v_c^j - v_c^i}{L}\right) \quad (67b)$$

$$\begin{aligned} \Delta w_c &= \left(1 - \frac{3x^2}{L^2} + \frac{2x^3}{L^3}\right) \Delta w_c^i - \left(x - \frac{2x^2}{L} + \frac{x^3}{L^2}\right) \Delta\theta_y^i \\ &+ \left(\frac{3x^2}{L^2} - \frac{2x^3}{L^3}\right) \Delta w_c^j - \left(-\frac{x^2}{L} + \frac{x^3}{L^2}\right) \Delta\theta_y^j \end{aligned} \quad (67c)$$

$$\begin{aligned} \theta_x &= \left(1 - \frac{3x^2}{L^2} + \frac{2x^3}{L^3}\right) \theta_x^i + \left(x - \frac{2x^2}{L} + \frac{x^3}{L^2}\right) \theta_{x,x}^i \\ &+ \left(\frac{3x^2}{L^2} - \frac{2x^3}{L^3}\right) \theta_x^j + \left(-\frac{x^2}{L} + \frac{x^3}{L^2}\right) \theta_{x,x}^j \end{aligned} \quad (67d)$$

Inserting eq. (67) into eq. (65) gives:

$$-\Delta u_0 - h\theta_z = (-\Delta u_0^i - h\theta_z^i) \left(1 - \frac{x}{L}\right) + 3h \left(\frac{x}{L} - \frac{x^2}{L^2}\right) \left(\theta_z^i + \theta_z^j - 2\frac{v_c^j - v_c^i}{L}\right) = 0 \quad (68a)$$

$$\begin{aligned} -\Delta w_c + h\theta_x &= \left(1 - \frac{3x^2}{L^2} + \frac{2x^3}{L^3}\right) (-\Delta w_c^i + h\theta_x^i) + \left(\frac{3x^2}{L^2} - \frac{2x^3}{L^3}\right) (-\Delta w_c^j + h\theta_x^j) \\ &+ \left(x - \frac{2x^2}{L} + \frac{x^3}{L^2}\right) (\Delta\theta_y^i + h\theta_{x,x}^i) + \left(-\frac{x^2}{L} + \frac{x^3}{L^2}\right) (\Delta\theta_y^j + h\theta_{x,x}^j) = 0 \end{aligned} \quad (68b)$$

Inserting eq. (66) into eq. (68a), the element degrees of freedom are found to be constrained through the following condition:

$$\theta_z^i + \theta_z^j = 2\frac{v_c^j - v_c^i}{L} \quad (69)$$

Combining eq. (69) and eq. (67b), the variation of  $\theta_z$  along the element, initially described by a quadratic polynomial, changes into a first-order one. As a result, the beam curvature becomes constant within the element. This behavior has been referred to curvature or slip-locking [16, 17, 18].

Besides, it is interesting to note that in contrast to zero longitudinal slip state, the zero lateral slip (65b) provides no additional kinematic constraint. This difference can be traced back to the use of Hermite interpolation function for the twisting angle  $\theta_x$  and linear interpolation function for the axial displacements  $u_0^a$  and  $u_0^b$ .

To prevent slip-locking, the composite beam element has been upgraded from 20 degrees of freedom (DOFs) to 22 DOFs by adding two DOFs at the middle of the element. The additional DOFs are related to the axial displacements of the beam (a) and (b). Thus, the interpolation function for the axial displacements can be expressed as:

$$u_0 = u_0^i + \frac{4u_0^m - u_0^j - 3u_0^i}{L}x + \frac{u_0^j - 2u_0^m + u_0^i}{L^2}2x^2 \quad (70)$$

where  $u_0^m$  is the additional degree of freedom associated to the axial displacement at the middle of the beam. By using the new interpolation function of eq. (70), the zero-slip constraint will produce the following condition:

$$\Delta u_0^i + \Delta u_0^j + 4\Delta u_0^m = \frac{6}{L} (v_c^i - v_c^j) h \quad (71)$$

By refining the composite beam element, we removed the constraint imposed by eq. (69) on the interpolation function for the rotation  $\theta_z$ , which results in a locking-free formulation.

## 8. Examples and comparisons

### 8.1. Example 1: A cantilever beam subjected to concentrated loads

Schnabl and Planinc [13] derived a closed-form solution for a linear elastic 3D composite beam. They assumed an Euler-Bernoulli beam theory for both layers and neglected warping effects. At the contact area, the layers are supposed to be continuously connected using adhesive bonding with finite stiffness. In addition, the uplift is not allowed. Therefore, the composite beam can only experience horizontal slip in two directions.

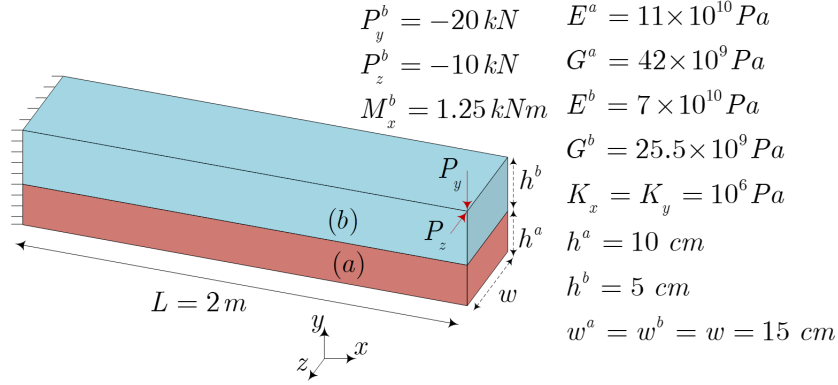


Figure 5: Cantilever beam subjected to concentrated loading case

We consider a cantilever composite beam consisting of two connected rectangular layers (see fig. 5) and subjected to a combination of vertical and horizontal point loads at the free end. A single row of deformable connectors is positioned at the  $XY$ -plane of symmetry of the composite section. The connectors are assumed to be linear elastic with an equivalent stiffness in two directions.

Table 1: Numerical results of the slip in the  $XY$ -plane

$-\Delta u_0 - h \theta_z$	$x = 0$	$x = L/4$	$x = L/2$	$x = 3L/4$	$x = L$
[13]	0	0.0876	0.1501	0.1875	0.2 (cm)
DMWW	0	0.0876	0.1501	0.1875	0.2 (cm)
DMNW	0	0.0876	0.1501	0.1875	0.2 (cm)

Table 2: Numerical results of the slip in the  $XZ$ -plane

$-\Delta w_c + h \theta_x$	$x = 0$	$x = L/4$	$x = L/2$	$x = 3L/4$	$x = L$
[13]	0	0.0717	0.2821	0.6170	1.0369 (cm)
DMWW	0	0.0729	0.2842	0.6201	1.0417 (cm)
DMNW	0	0.0726	0.2836	0.6193	1.0406 (cm)

To assess the influence of warping effects on the composite beam response, two finite element models were considered: DMWW (Direct method presented in section 5) and DMNW

(Direct method without warping presented in Appendix A). As the exact formulation provides accurate results, a single finite element is sufficient to analyze the response of the composite beam using the two models.

In table 1 and table 2, the values of slips in both directions obtained with both models are compared against the results of Schnabl and Planinc [13]. It can be seen that there is an excellent agreement regarding the longitudinal slip. Besides, there are some slight differences in term of lateral slip. Despite ignoring the warping effects in the DMNW model, the lateral slip obtained are slightly different compared to the presented results in [13]. In fact, these small differences can be originated from our consideration of a discrete shear connection in the lateral direction in both models.

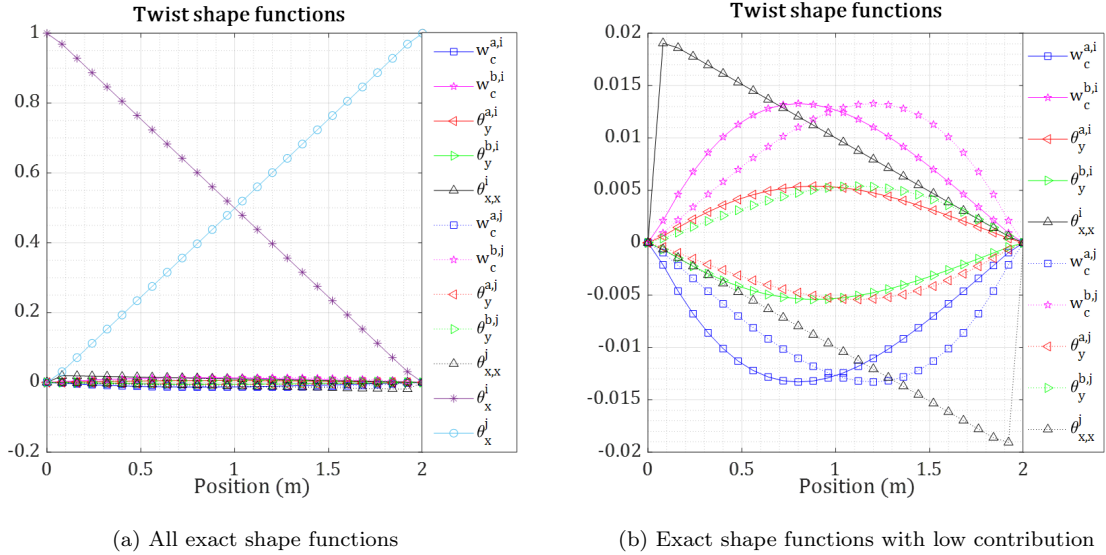


Figure 6: Twist angle shape functions

To acquire a deeper understanding of the performance of the proposed formulation (DMWW), we evaluate the contribution of all DOFs responsible for the torsional response of the composite beam, see Figure 6. It can be seen that apart from  $\theta_x^i$  and  $\theta_x^j$ , the remaining DOFs do not contribute significantly. Therefore, the neglecting warping effects is acceptable for this considered example. Furthermore, referring to fig. 6a, the twist angle can be approximated using linear interpolation functions.

## 8.2. Example 2: Locking problem in displacement-based formulation

In this example, we investigate the influence of connection rigidity on the response of the composite beam. The previously used composite beam geometry (fig. 5) is adopted. The objective is to evaluate the performance of the displacement-based formulation (DBM) with regards to the exact solution (DM), particularly with high connection stiffness. Both DBM with 20 DOFs (DBM20) and 22 DOFs (DBM22) are evaluated. The analysis is performed with 5, 10 and 20 elements for DBM20 and DBM22 models, while only one single element is used for DM model. The evolution of the maximum interlayer slips at the tip of the composite beam obtained with the exact formulation in function of the connection stiffness are depicted in fig. 7. It can be seen in fig. 7a that the longitudinal slip is not altered by the change of the lateral connection stiffness  $K_z$ . Similarly, the lateral slip is not impacted by the longitudinal connection stiffness  $K_x$  (see fig. 7b). It can be noted that for values of  $K_x$  and  $K_z$  higher than  $10^{10}$  Pa, both longitudinal and lateral slips approach zero. It is worth recalling that the connectors are placed along the vertical axis of symmetry where warping deformations vanish. Consequently, the influence of the connection stiffness in both directions is uncoupled and can be studied independently.

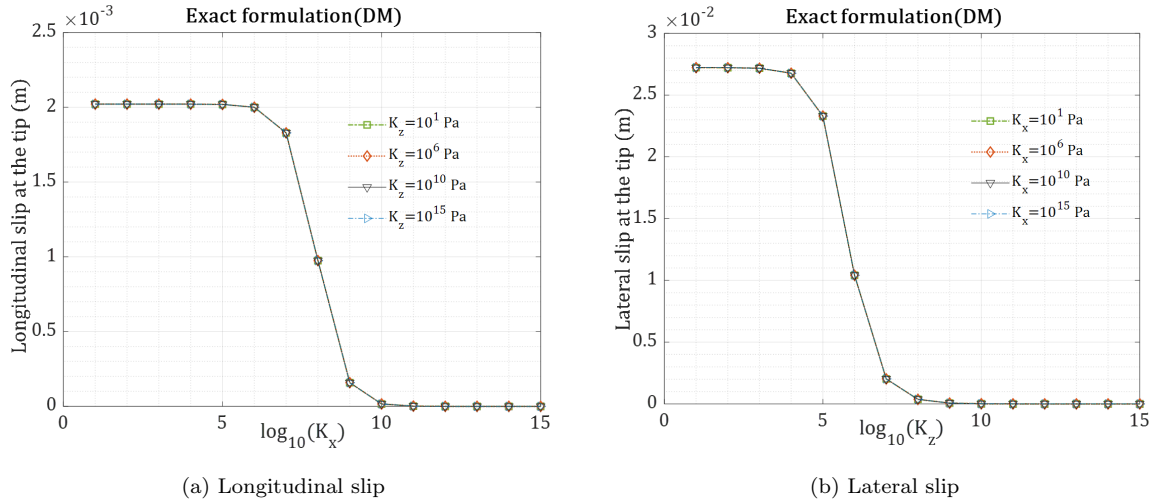


Figure 7: Maximum inter-layer slips versus connection stiffness

The ratio between the slip obtained with DBM and the maximum slip at the tip obtained

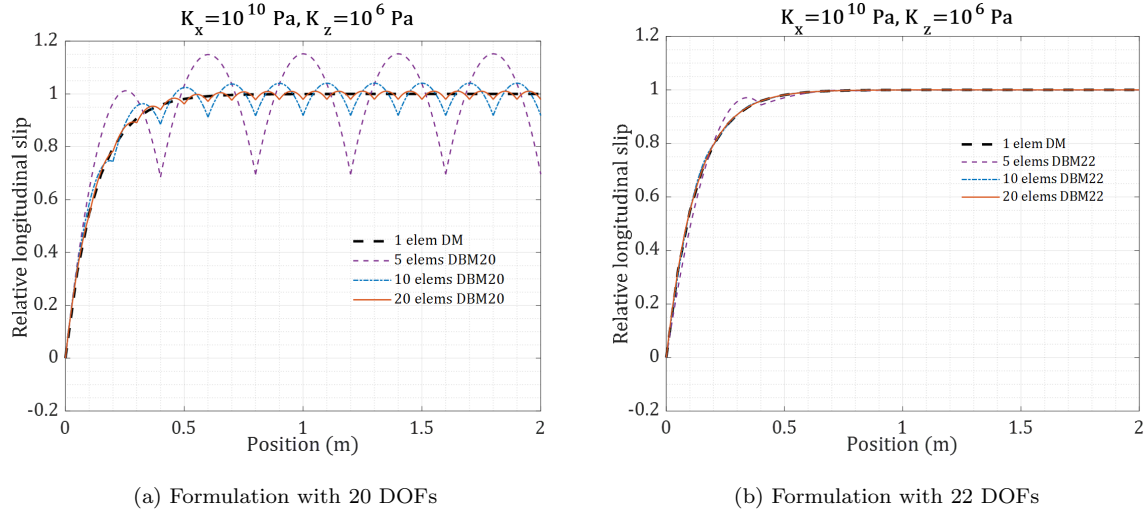


Figure 8: The evolution of the relative longitudinal slip for DBM20 and DBM22 formulations

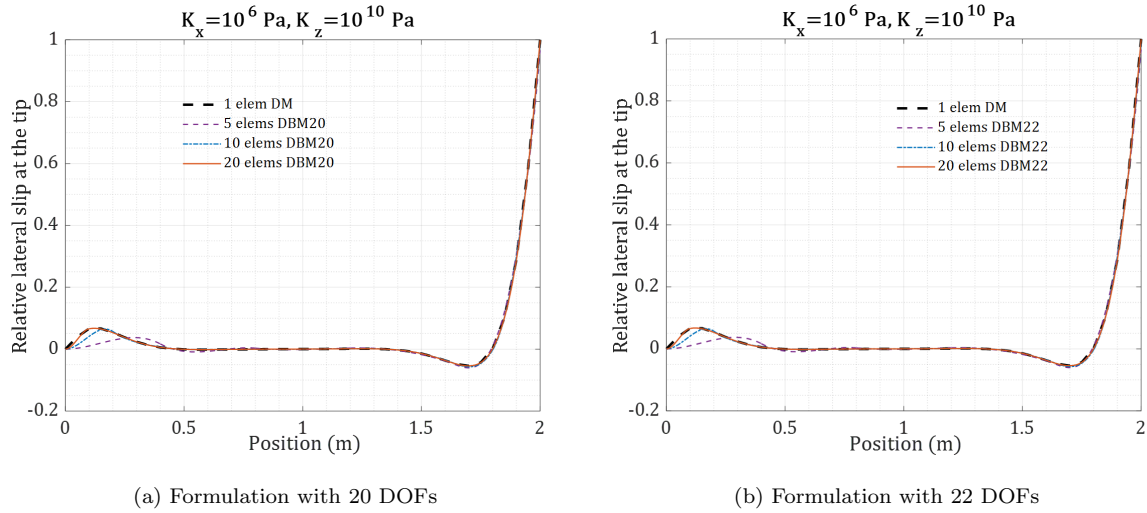


Figure 9: The evolution of the relative lateral slip for DBM20 and DBM22 formulations

with DM is depicted in Figure 8a. It is worth mentioning that the interpolation functions are used to evaluate the slip distribution between the element ends. We observe an oscillatory behavior of the longitudinal slip distribution obtained with DBM20 model when a high connection rigidity ( $K_x = 10^{10}$  Pa) is considered, see fig. 8a. Using a finer mesh (10 and 20 elements), locking effects are reduced and the response of DBM20 model is gradually approaching that of the DM model. On the other hand, DBM22 model predictions are in good agreement with that of the DM model. Regarding the lateral slip, no locking problem

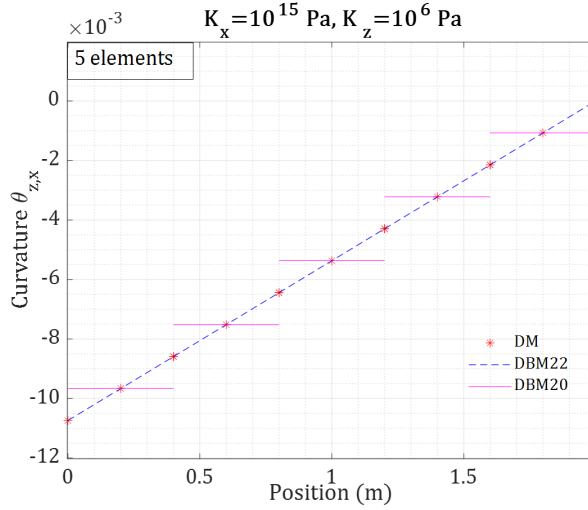


Figure 10: The curvature of the composite beam in the  $XY$ -plane for  $K_x = 10^{15}$  Pa and  $K_z = 10^6$  Pa

is observed and the DBM20 and DBM22 models are capable of reproducing accurately the response of DM model with a finer mesh (above 10 elements), see fig. 9. The lateral deformation of the DBM20 and DBM22 models, is controlled by the same interpolation functions and DOFs (see section 7). Thus, the lateral slip evolutions predicted by the DBM20 and DBM22 models exhibit identical behaviors (see figs. 9a and 9b). Furthermore, to have a better insight into the locking problem issue, we consider an even higher connection rigidity ( $K_x = 10^{15}$  Pa). Five DBM20 and DBM22 elements are considered. It results in a constant curvature  $\theta_{z,x}$  within every DBM20 single element, as depicted in fig. 10. According to figs. 9b and 10, it is clear that the DBM22 model is capable of reproducing, accurately, the composite beam curvature while avoiding slip-locking.

### 8.3. Example 3: A cantilever composite beam subjected to distributed torsional moment

In the following example, a 2 m cantilever composite beam subjected to a uniformly distributed torsional moment (100 N.m/m) will be studied. The cross-section is made of an HEA140 steel profile connected to a  $180 \times 500$  mm concrete slab. The characteristics of the composite section are presented in fig. 11. The interface connection is provided by two rows of shear connectors with two directional connection rigidity,  $K_x = 10^6$  Pa and  $K_z = 10^6$  Pa.

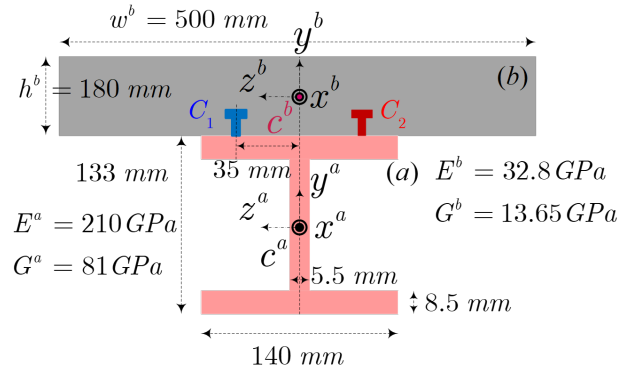


Figure 11: I-steel-concrete composite beam

For this specific example, the exact formulation is adopted, using a single finite element. Except warping, all displacements are prevented at the clamped end. The composite beam will be analyzed using both DMWW and DMNW models in order to evaluate the influence of warping effects on the beam response. Figure 12 presents the distributed shear forces in the connector in both directions. It appears that taking warping effects into consideration results in a significant increase in the connection shear forces. Furthermore, due to warping the longitudinal slip at the clamped section is not zero, resulting a non zero longitudinal shear force at clamped section. Additionally, warping also affects the internal forces, particularly

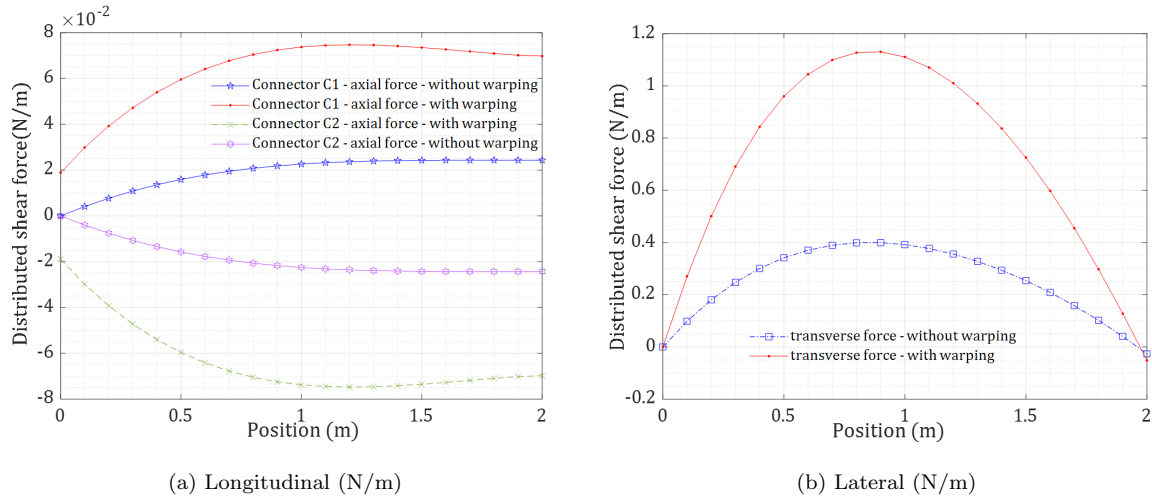


Figure 12: Distributed shear forces in the connectors (N/m)

the lateral bending moments (see fig. 13). It is due to the fact that the longitudinal shear force has been augmented when considering the warping effects. To equilibrate this shear force the lateral bending moment has to be increased. As a result, it is observed that the highest axial stress in the composite section obtained with DMWW model is more than doubled compared to that obtained with DMNW model (see figs. 14a and 14b). It can be seen in figs. 14a and 14b that the axial stress in the concrete slab is much lower than the one in the steel profile ( $\frac{\sigma_x^{b,\max}}{\sigma_x^{a,\max}} = 0.74\%$ ) which agrees very well with the ratio of their bending rigidities  $\frac{E^b I_y^b}{E^a I_y^a} = 75.08$ . Figures 15a and 15b represent, respectively, the shear stress distributions in both transverse direction ( $\tau_{xz}$  and  $\tau_{xy}$ ). It can be seen that the torsional shear stress flow for both  $\tau_{xz}$  and  $\tau_{xy}$  is concentrated at both the perimeter of the concrete slab and the steel profile. Additionally, both  $\tau_{xz}$  and  $\tau_{xy}$  fulfill the contour boundary conditions. On the other hand, when warping is restrained (warping DOF is blocked) at the support, the axial stress profile  $\sigma_x$  exhibits a different behavior. Indeed, the contour plot of the axial stress  $\sigma_x$  appears to be similar to the warping-generated axial stresses, as shown in fig. 16. It is worth noting that the maximum axial stress is ten times greater than the one obtained with the unrestrained warping case. Furthermore, the maximum axial stress on the concrete slab  $\sigma_x$  is comparable to that on the steel profile with a maximum stress ratio of  $\frac{\sigma_x^{b,\max}}{\sigma_x^{a,\max}} = 40.34\%$ . It is worth noting that the axial stress distribution is now influenced not only by lateral bending of the composite section but also by warping deformation (see fig. 16).

#### 8.4. Example 4: A cantilever composite beam subjected to a torsional moment

In this example, the same composite cantilever beam presented in the example (8.3) is considered. However, a 5 kNm torsional moment is applied at the free end, see Figure 17. Using the proposed DMWW model, a parametric study is performed to gain insight into the complex behavior of the composite beam subjected to a torsional moment. We focus on the slip distributions and analyze the influence of the connection rigidity as well as the warping effects on the composite beam response. To do so, we introduced two dimensionless parameters  $\alpha_u L$  and  $\alpha_\omega L^2$ , representing the connection rigidity in longitudinal and lateral

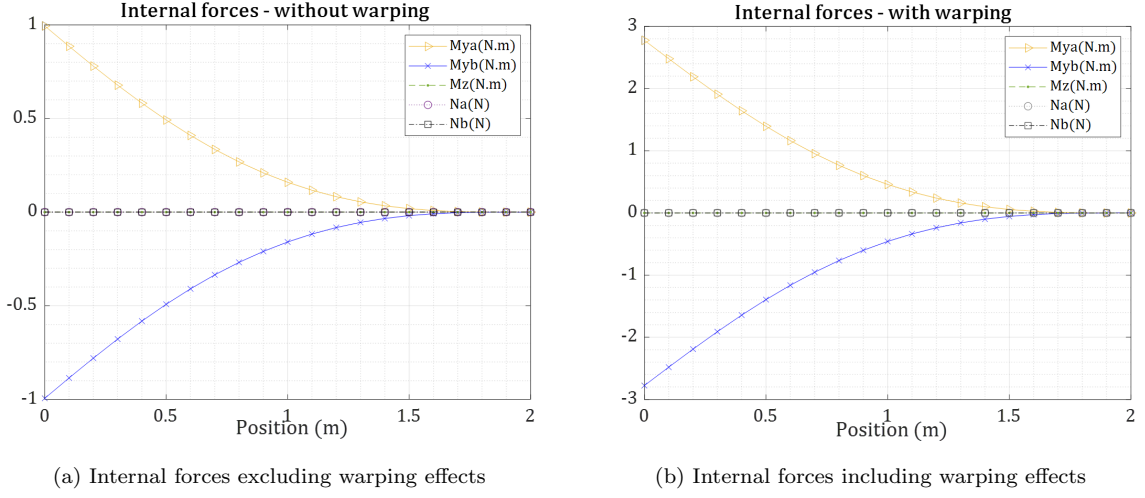


Figure 13: Internal forces

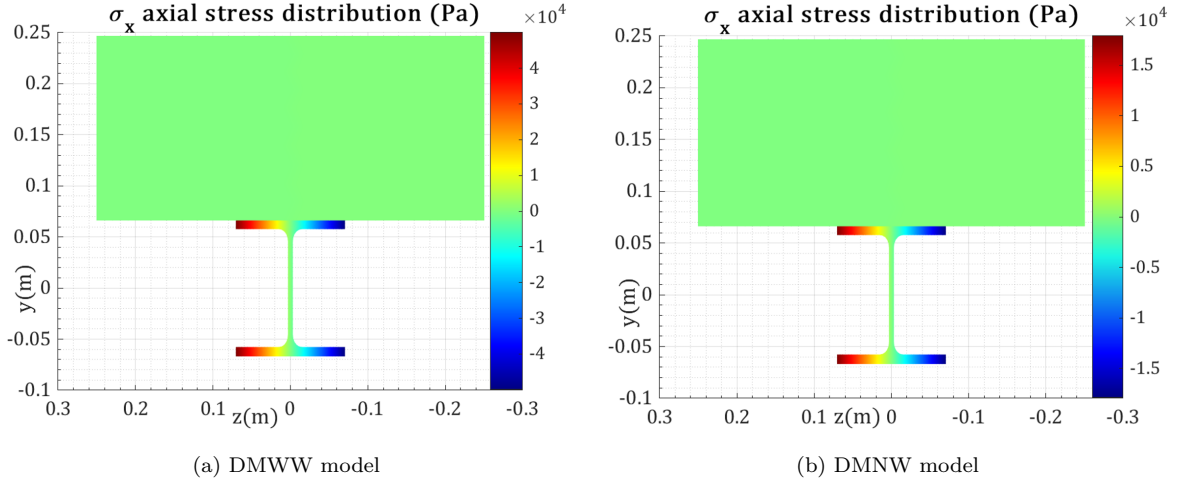


Figure 14: The  $\sigma_x$  axial stress distribution - unrestrained warping

direction, respectively, where:

$$\alpha_u^2 = 2nK_x \left( \frac{1}{EA} + \frac{h^2}{EI_z^s} \right) \quad (72a)$$

$$\alpha_w^2 = K_z \left( \frac{1}{EI_y} + \frac{h_c^2}{EI_w^s} \right) \quad (72b)$$

These two parameters  $\alpha_u$  and  $\alpha_w$  appear in the solution of the governing equations (Equations (34) and (42)). The same dimensionless parameter ( $\alpha_u L$ ) has been used in [21, 22, 23] to study partial interaction effects on the planar composite beam response. In the present

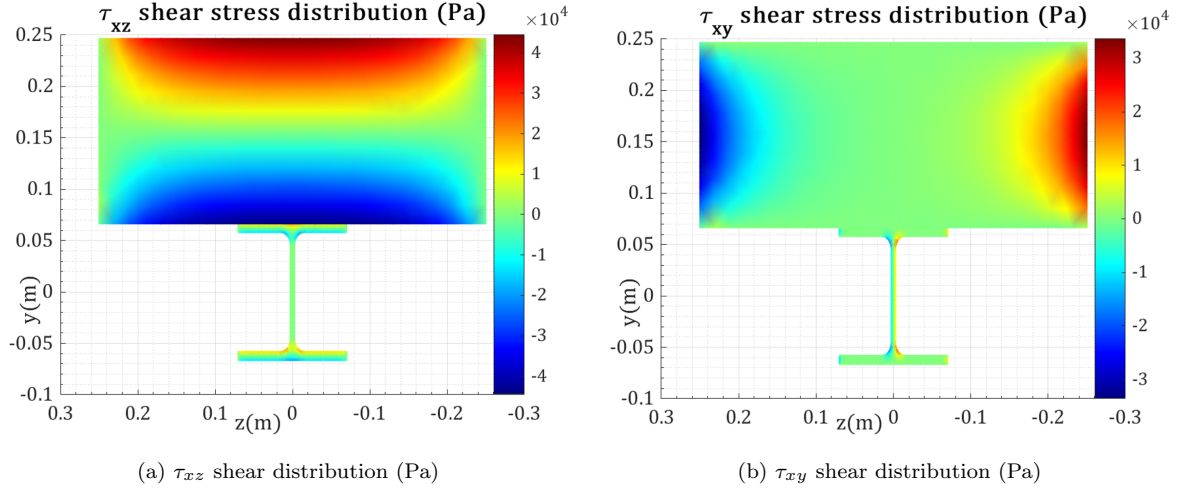


Figure 15: The cross-section shear distribution using DMWW model - unrestrained warping

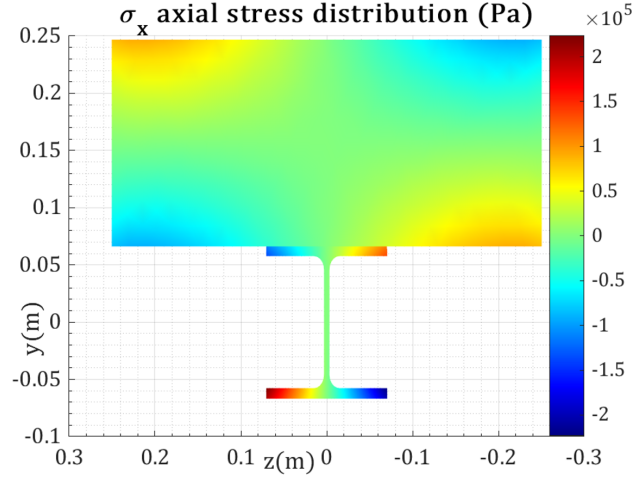


Figure 16: The  $\sigma_x$  axial stress distribution using DMWW model - restrained warping

model, a new additional parameter  $\alpha_\omega$  representing a semi-rigid connection in lateral direction, is featured and its effects on the partial interactions in both directions are examined. The expressions of longitudinal and lateral slips are recalled here:

$$s_{px} = -\Delta u_0 - h\theta_z - z_p \Delta\theta_y + \omega_p \theta_{x,x} \quad (73)$$

$$s_z = -\Delta w_c + h_c \theta_x \quad (74)$$

Before presenting the slip distributions, the parameters involved in the slip expressions are studied. It should be noted that one of the parameters  $\alpha_u L$  or  $\alpha_\omega L^2$  is fixed and the other

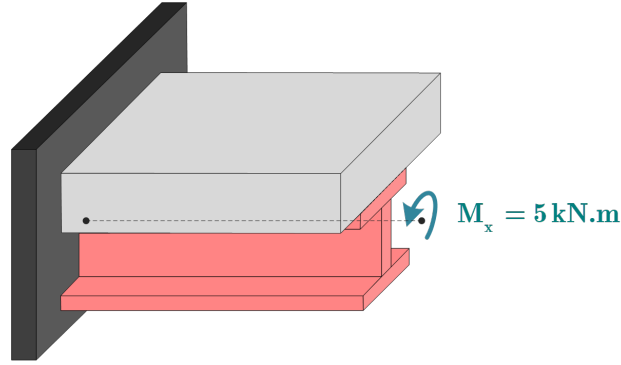


Figure 17: I-steel-concrete composite beam: load configuration

is varied, considering the following set:  $\{1, 2, 4, 6, 8, 10, 12, 14, 16, 18, 20\}$ . It is worth mentioning that a full interaction behavior can be obtained for  $\alpha_u L$  values exceeding 10 for 2D planar composite beam [21, 22, 23].

#### 8.4.1. Lateral shear force response

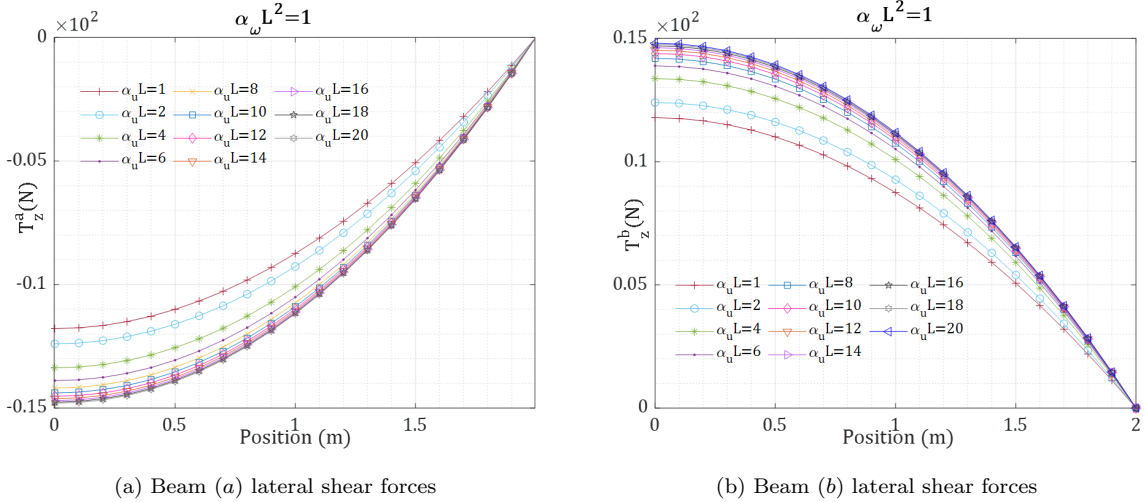
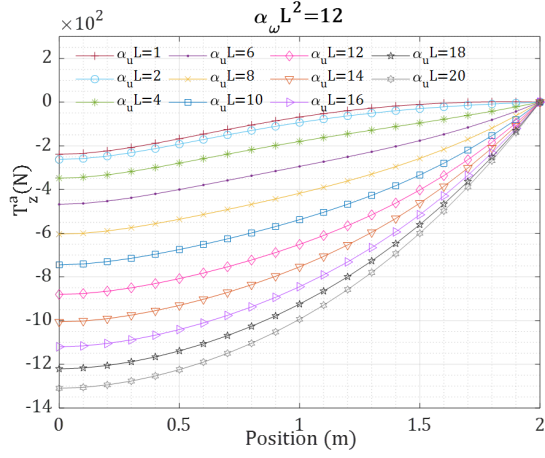
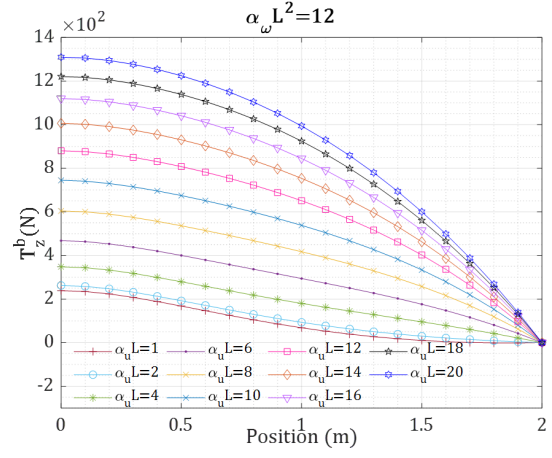


Figure 18: Distribution of the composite beam's lateral shear forces with  $\alpha_\omega L^2 = 1$

The influences of the longitudinal connection stiffness ( $\alpha_u L$ ) on the lateral shear forces in each layer for a low ( $\alpha_\omega L^2 = 1$ ) and high ( $\alpha_\omega L^2 = 12$ ) lateral connection rigidity are depicted in figs. 18 and 19, respectively. In case of low lateral connection stiffness (see fig. 18), increasing the longitudinal connection stiffness from  $\alpha_u L = 1$  to  $\alpha_u L = 20$  results in a 25% increase of the lateral shear forces values in both layer. However, they increase



(a) Beam (a) lateral shear forces

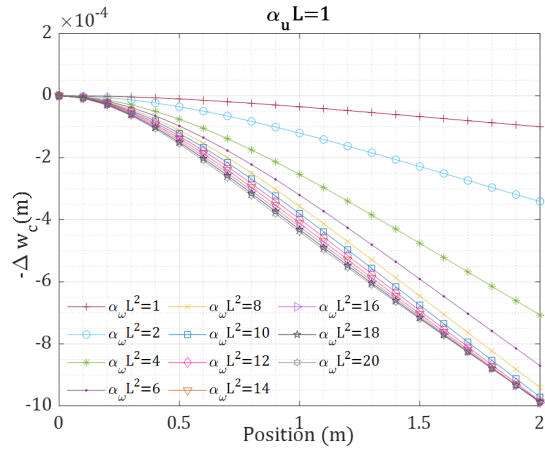


(b) Beam (b) lateral shear forces

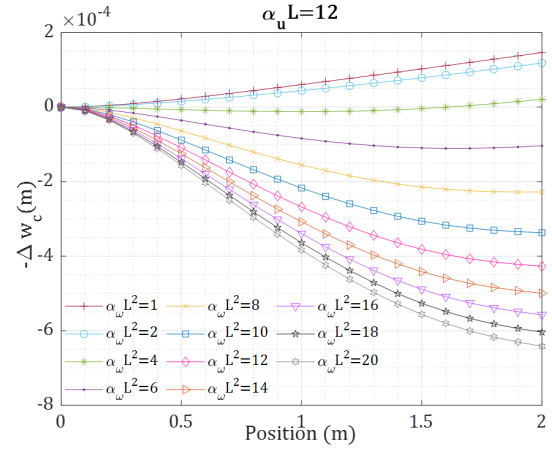
Figure 19: Distribution of the composite beam's lateral shear forces with  $\alpha_\omega L^2 = 12$

significantly with a high lateral connection stiffness, see fig. 19. It shows that a portion of the torsional moment is transferred as a couple of lateral shear forces applied at the respective shear center of each layer. The magnitude of those lateral shear forces are in function of the rigidity of the connection.

#### 8.4.2. Lateral displacement response



(a) Case of  $\alpha_u L = 1$



(b) Case of  $\alpha_u L = 12$

Figure 20: Partial interaction effects on the difference of the two lateral displacements  $-\Delta w_c$

Figure 20 illustrates the influence of  $\alpha_\omega L^2$  on the difference of lateral displacements

( $-\Delta w_c = w_c^a - w_c^b$ ) of the two layers. As expected, when  $\alpha_\omega L^2$  increases,  $-\Delta w_c$  decreases. Besides, it can be seen that with a loose longitudinal connection (see fig. 20a), the lateral displacement of layer (a) is lesser than that of layer (b). However, with a rigid longitudinal connection (see fig. 20b), the lateral displacement of layer (a) is greater than that of layer (b) for a low lateral connection stiffness. Nevertheless, the lateral displacement of layer (a) becomes smaller than that of layer (b) for a high lateral connection stiffness. It shows clearly that not only the rigidity of the lateral connection but also the stiffness of longitudinal connection influences the response of lateral displacement of each layer.

#### 8.4.3. Lateral rotation response

The influence of  $\alpha_u L$  on the value of  $\Delta\theta_y$ , in which  $\Delta\theta_y = \theta_y^b - \theta_y^a$ , is presented in fig. 21. It can be seen that  $\Delta\theta_y$  increases with increasing value of  $\alpha_u L$  for both low and high lateral connection stiffness. However, for a high value of  $\alpha_u L$ , the distribution of  $\Delta\theta_y$  with  $\alpha_\omega L^2 = 1$  is completely different from that with  $\alpha_\omega L^2 = 12$ . This may be explained by the change of  $-\Delta w_c$  distribution from almost linear for  $\alpha_\omega L^2 = 1$  to non-linear curve for  $\alpha_\omega L^2 = 12$  as depicted in fig. 20b.

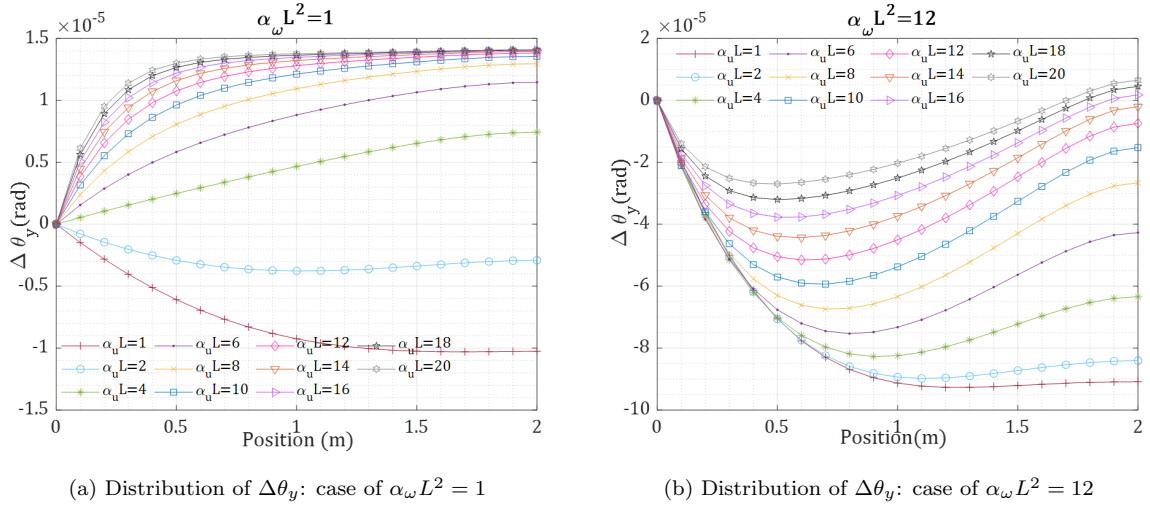


Figure 21: Partial interaction effects on the response of  $\Delta\theta_y$

#### 8.4.4. Torsional rotation and its derivative response

Figures 22 and 23 shows the partial interaction effects on the response of  $\theta_x$  and  $\theta_{x,x}$ , respectively. It can be seen that the distribution of torsional rotation  $\theta_x$  is almost linear and insignificantly influenced by the connection stiffness. As a result, its derivative  $\theta_{x,x}$  is nearly constant.

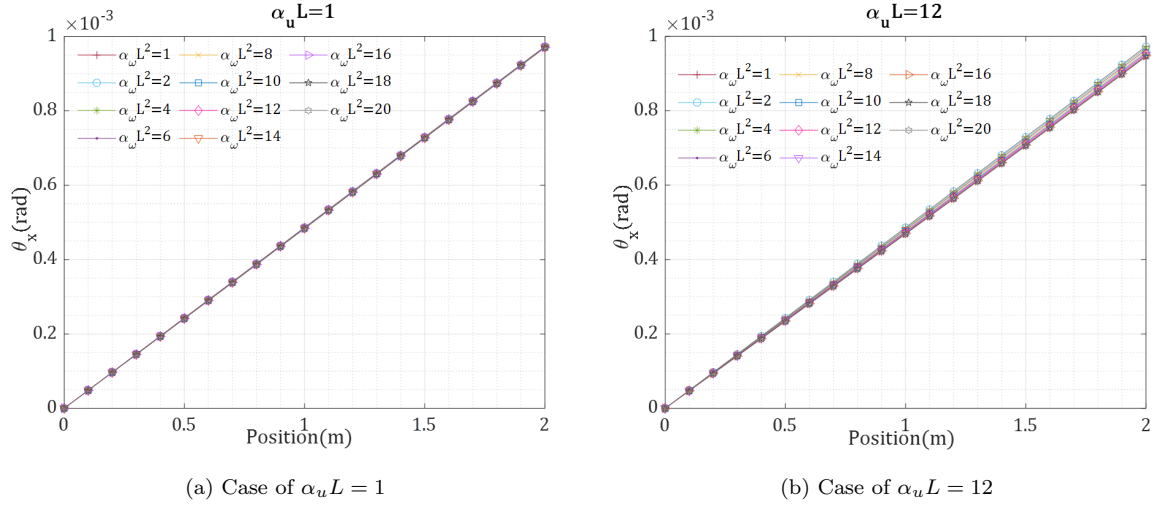


Figure 22: Partial interaction effects on the response of  $\theta_x$

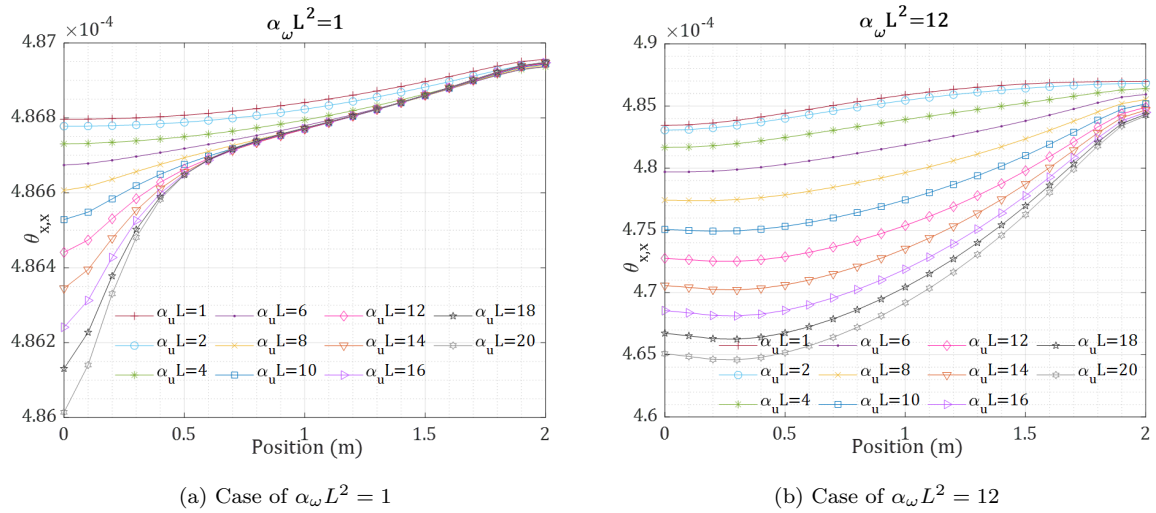


Figure 23: Partial interaction effects on the response of  $\theta_{x,x}$

#### 8.4.5. Longitudinal relative slip $\bar{s}_{rx}$

Figure 24 illustrates the effects of the connection rigidity on the distribution of the relative longitudinal slip at the connector  $C_1$  (see fig. 11). It is worth mentioning that the two graphs represent two parametric studies and in each graph, the slip is normalized with respect to the highest value obtained for each parametric study. For a low lateral connection

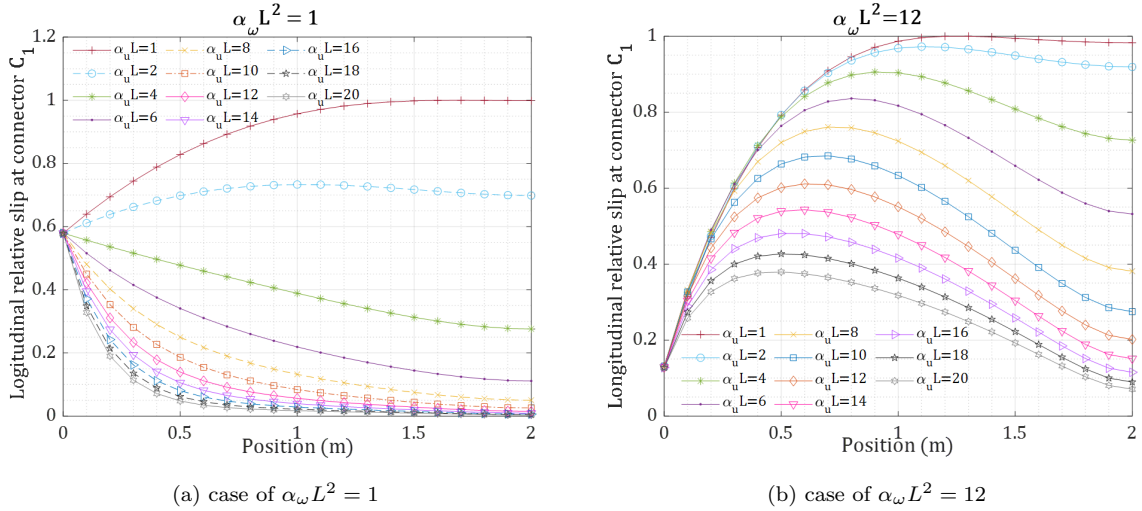


Figure 24: Distribution of the relative longitudinal slip

stiffness ( $\alpha_\omega L^2 = 1$ , see fig. 24a), the maximum longitudinal slip is obtained at the free end of the composite beam when a loose longitudinal connection is considered ( $\alpha_u L = 1$ ). With a high longitudinal connection stiffness, the longitudinal slip at the free end decreases and tends to zero. However, regardless of the longitudinal connection rigidity, it maintains nearly the same non-zero value at the support where only warping is allowed. It shows clearly that the cross-sectional warping has an effect on the distribution of the longitudinal slip. When a high lateral connection rigidity is considered ( $\alpha_\omega L^2 = 12$ , see fig. 24b), the distribution of the longitudinal slip exhibits a different behavior. The maximum longitudinal slip is obtained at the intermediate point between support and free end of the composite beam. It is interesting to note that even with higher longitudinal connection stiffness ( $\alpha_u L = 20$ ), significant values of  $\bar{s}_{rx}$  are still observed along the beam length. In fact, with a higher lateral connection rigidity, a larger lateral shear force is produced at the shear center of the

layer, see figs. 18 and 19. Due to different cross-section rigidities of the layers and different distances of the shear centers to the connection surface, the difference of lateral rotations  $\Delta\theta_y$  is obtained, see fig. 21. As a result, the longitudinal slip is produced, see eq. (73).

#### 8.4.6. Lateral relative slip $\bar{s}_{rz}$

The effects of partial interaction on the lateral slip response are illustrated in fig. 25. For a low longitudinal connection stiffness ( $\alpha_u L = 1$ ),  $\bar{s}_{rz}$  experiences a rapid decrease as the parameter  $\alpha_\omega L^2$  increases. In fact, a 95% decrease in the value of  $\bar{s}_{rz}$  at the tip of the cantilever is recorded for  $\alpha_\omega L^2 = 8$  (see fig. 25a). Furthermore, a full lateral connection is nearly achieved for  $\alpha_\omega L^2 = 20$ , with some small values for  $\bar{s}_{rz}$  near the support region. In case of a high longitudinal connection rigidity ( $\alpha_u L = 12$ ), the distribution of  $\bar{s}_{rz}$  exhibits a different response with increasing  $\alpha_\omega L^2$ . Even with a high lateral connection stiffness ( $\alpha_\omega L^2 = 20$ ), a non-zero value for  $\bar{s}_{rz}$  is still observed at the beam's free end, as well as near the support region. By recalling eq. (74), the combination of  $-\Delta w_c$  and  $\theta_x$  defines the

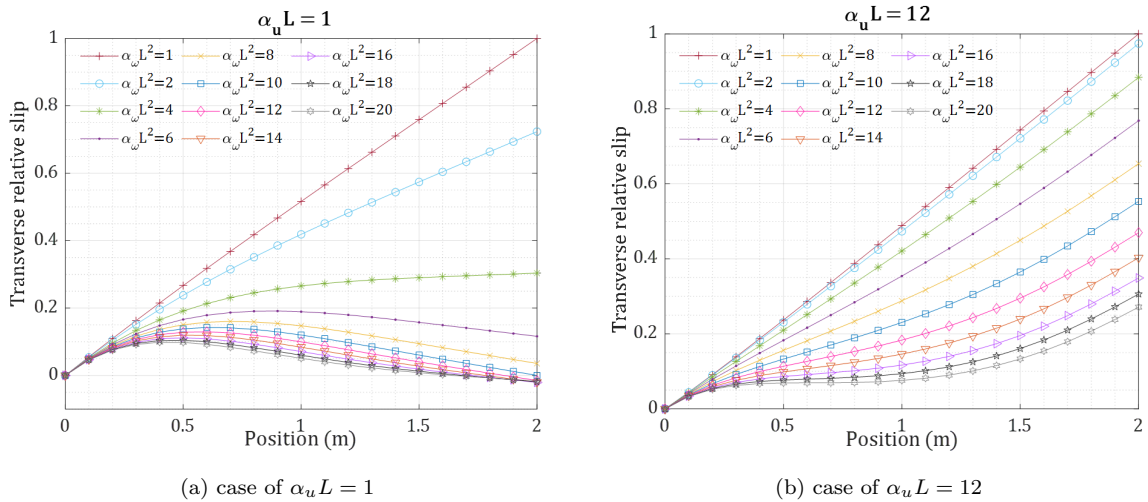


Figure 25: Distribution of the relative lateral slip

evolution of the lateral slip. Referring to figs. 20a and 20b, a strong correlation between  $\bar{s}_{rz}$  and  $-\Delta w_c$  is observed. Actually, a linear behavior of torsional rotation  $\theta_x$  is noted and is relatively identical for all the considered connection stiffness (see figs. 22a and 22b). Therefore,  $\bar{s}_{rz}$  is directly influenced by the distribution of  $\Delta w_c$ . Similarly to  $\Delta\theta_y$ , the presence

of  $-\Delta w_c$  can only be explained by the existence of the lateral shear forces whose intensities are functions of the connection stiffness.

## 9. Conclusions

In this paper, a new formulation has been developed to study mono-symmetric composite beams with deformable connection under general load conditions considering a non-uniform torsion. The assumption that shear connection has no influence on the warping of each subsection of the composite section has simplified significantly the formulation. In fact, the governing equilibrium equations in the primary plane (XY) become uncoupled from that of secondary plane (XZ). As a result, the closed-form solution can be obtained. Additionally, the direct stiffness method has been fully detailed accounting for the contributions of warping generated forces, as well as the interface shear forces in two directions. It has been shown that if the warping effects are neglected, it can significantly underestimate the composite beam's internal forces. Besides, a displacement-based formulation has been suggested as an alternative to the direct stiffness method. In case of a high shear connection, slip-locking occurs, when using a linear shape function for axial displacement fields, and the curvature becomes constant within the element. To overcome this issue, the axial displacement distributions were refined by additional two degrees of freedom at the middle of each layer. In addition, the connection stiffness has been found to affect the slip distribution at the interface, especially, when considering warping effects on the composite beam response.

For future developments, the effect of the connection stiffness on the warping shape of the composite section should be taken into account in order to account for the coupling between the displacement fields in the longitudinally symmetric plan and the orthogonal transverse plan, as well as the warping contribution to the stress resultants of each subsection.

## Appendix A. Composite beam theory without warping

Similarly to the development of section 5, the non-consideration of warping deformation will further simplify the governing equilibrium equations and the determination of the stiffness matrix of the element. Therefore, the system of eq. (32) becomes:

$$E^a A^a u_{0,xx}^a - \sum_{p=1}^{2n} K_{px} (-\Delta u_0 - h \theta_z) + n_x^a = 0 \quad (\text{A.1a})$$

$$E^b A^b u_{0,xx}^b + \sum_{p=1}^{2n} K_{px} (-\Delta u_0 - h \theta_z) + n_x^b = 0 \quad (\text{A.1b})$$

$$(E^a I_z^a + E^b I_z^b) \theta_{z,xxx}^a + \sum_{p=1}^{2n} h K_{px} (-\Delta u_{0,x} - h \theta_{z,x}) = q_y^a + q_y^b \quad (\text{A.1c})$$

$$E^a I_y^a \theta_{y,xxx}^a - K_z (-\Delta w_c + h_c \theta_x) + \sum_{p=1}^{2n} z_p^2 K_{px} \Delta \theta_{y,x} + q_z^a = 0 \quad (\text{A.1d})$$

$$E^b I_y^b \theta_{y,xxx}^b + K_z (-\Delta w_c + h_c \theta_x) - \sum_{p=1}^{2n} z_p^2 K_{px} \Delta \theta_{y,x} + q_z^b = 0 \quad (\text{A.1e})$$

$$(G^a J^a + G^b J^b) \theta_{x,xx} - h_c K_z (-\Delta w_c + h_c \theta_x) + m_x = 0 \quad (\text{A.1f})$$

The equations (A.1a, A.1b, A.1c), are exactly the same as in case of non-uniform-torsion, therefore, the system solution in  $XY$ -plane will be the same as introduced in section 5.1.1. Using the last equations (A.1d, A.1e, A.1f), the compact format of the  $XZ$ -plane can be formulated as follows:

$$\begin{aligned} & \frac{\overline{GJ}^s}{h_c K_z} \theta_x^{(6)} - \left( h_c + \frac{K_x}{h_c K_z} \frac{\overline{GJ}^s}{\overline{EI}_y} \sum_{p=1}^{2n} z_p^2 \right) \theta_x^{(4)} + \left( \frac{\overline{GJ}^s}{\overline{EI}_y h_c} + \frac{K_x}{\overline{EI}_y} h_c \sum_{p=1}^{2n} z_p^2 \right) \theta_x^{(2)} \\ & + \frac{1}{h_c \overline{EI}_y} m_x + \frac{q_z^b}{E^b I_y^b} - \frac{q_z^a}{E^a I_y^a} = 0 \end{aligned} \quad (\text{A.2})$$

Consequently, the system's solution can be written in the following format:

$$\theta_x = C_9 e^{r_1 x} + C_{10} e^{r_2 x} + C_{11} e^{r_3 x} + C_{12} e^{r_4 x} + C_{13} e^{r_5 x} + C_{14} e^{r_6 x} + \theta_x^p \quad (\text{A.3})$$

where

$$\theta_x^p = \frac{-1}{\overline{GJ}^s + K_x h_c^2 \sum_{p=1}^{2n} z_p^2} \frac{x^2}{2} \left( m_x + h_c \frac{\overline{EI}_y q_z^b}{E^b I_y^b} - h_c \frac{\overline{EI}_y q_z^a}{E^a I_y^a} \right) \quad (\text{A.4})$$

is the particular solution of the twist angle function and  $r_1, r_2, \dots, r_6$  are the roots of the following characteristic equation:

$$\left[ \frac{\overline{GJ}^s}{h_c K_z} r^4 - \left( h_c + \frac{K_x \overline{GJ}^s}{h_c K_z \overline{EI}_y} \sum_{p=1}^{2n} z_p^2 \right) r^2 + \left( \frac{\overline{GJ}^s}{\overline{EI}_y h_c} + \frac{K_x}{\overline{EI}_y} h_c \sum_{p=1}^{2n} z_p^2 \right) \right] r^2 = 0 \quad (\text{A.5})$$

Using the expression of  $\theta_x$  both  $w_s^a$  and  $w_s^b$  can be derived on the basis of the built relationships in eq. (A.1). The determination of the element stiffness matrix is obtained similarly to the one introduced in section 5.3.

## References

- [1] Q.-H. Nguyen, M. Hjiaj, S. Guezouli, Exact finite element model for shear-deformable two-layer beams with discrete shear connection, *Finite elements in analysis and design* 47 (2011) 718–727.
- [2] N. M. Newmark, Test and analysis of composite beam with incomplete interaction, *proc. of society for experimental stress Analysis* (1991) 75–92.
- [3] C. Faella, E. Martinelli, E. Nigro, Steel and concrete composite beams with flexible shear connection: “exact” analytical expression of the stiffness matrix and applications, *Computers & structures* 80 (2002) 1001–1009.
- [4] U. A. Girhammar, V. K. Gopu, Composite beam-columns with interlayer slip—exact analysis, *Journal of Structural Engineering* 119 (1993) 1265–1282.
- [5] U. A. Girhammar, D. H. Pan, Exact static analysis of partially composite beams and beam-columns, *International Journal of Mechanical Sciences* 49 (2007) 239–255.
- [6] P. Keo, Q.-H. Nguyen, H. Somja, M. Hjiaj, Derivation of the exact stiffness matrix of shear-deformable multi-layered beam element in partial interaction, *Finite Elements in Analysis and Design* 112 (2016) 40–49.
- [7] Q.-H. Nguyen, E. Martinelli, M. Hjiaj, Derivation of the exact stiffness matrix for a two-layer timoshenko beam element with partial interaction, *Engineering Structures* 33 (2011) 298–307.
- [8] G. Ranzi, M. Bradford, B. Uy, A direct stiffness analysis of a composite beam with partial interaction, *International Journal for Numerical Methods in Engineering* 61 (2004) 657–672.
- [9] P. Foraboschi, Analytical solution of two-layer beam taking into account nonlinear interlayer slip, *Journal of engineering mechanics* 135 (2009) 1129–1146.
- [10] Y. Wu, D. Oehlers, M. Griffith, Partial-interaction analysis of composite beam/column members, *Mechanics of Structures and Machines* (2007).
- [11] R. Xu, Y. Wu, Static, dynamic, and buckling analysis of partial interaction composite members using timoshenko’s beam theory, *International Journal of Mechanical Sciences* 49 (2007) 1139–1155.
- [12] A. Adekola, Partial interaction between elastically connected elements of a composite beam, *International Journal of Solids and Structures* 4 (1968) 1125–1135.
- [13] S. Schnabl, I. Planinc, Three-dimensional bimetallic layered beams with interface compliance: Analytical solution, *Proceedings of the Institution of Mechanical Engineers, Part L: Journal of Materials: Design and Applications* 233 (2019) 358–371.
- [14] A. Dall’Asta, Composite beams with weak shear connection, *International Journal of Solids and Structures* 38 (2001) 5605–5624.
- [15] S. Schnabl, M. Saje, G. Turk, I. Planinc, Locking-free two-layer timoshenko beam element with interlayer slip, *Finite Elements in Analysis and Design* 43 (2007) 705–714.

- [16] A. Dall'Asta, A. Zona, Slip locking in finite elements for composite beams with deformable shear connection, *Finite Elements in Analysis and Design* 40 (2004) 1907–1930.
- [17] R. E. Erkmen, M. A. Bradford, Treatment of slip locking for displacement-based finite element analysis of composite beam–columns, *International journal for numerical methods in engineering* 85 (2011) 805–826.
- [18] G. Ranzi, Locking problems in the partial interaction analysis of multi-layered composite beams, *Engineering Structures* 30 (2008) 2900–2911.
- [19] J. S. Dai, Euler–rodriques formula variations, quaternion conjugation and intrinsic connections, *Mechanism and Machine Theory* 92 (2015) 144–152.
- [20] R. Wituła, D. Słota, Cardano’s formula, square roots, chebyshev polynomials and radicals, *Journal of Mathematical Analysis and Applications* 363 (2010) 639–647.
- [21] C. Faella, E. Martinelli, E. Nigro, Steel and concrete composite beams with flexible shear connection: “exact” analytical expression of the stiffness matrix and applications, *Computers & Structures* 80 (2002) 1001–1009.
- [22] C. Faella, E. Martinelli, E. Nigro, Steel–concrete composite beams in partial interaction: Closed-form “exact” expression of the stiffness matrix and the vector of equivalent nodal forces, *Engineering Structures* 32 (2010) 2744–2754.
- [23] E. Martinelli, Q. H. Nguyen, M. Hjiiaj, Dimensionless formulation and comparative study of analytical models for composite beams in partial interaction, *Journal of Constructional Steel Research* 75 (2012) 21–31.